Status report of the CAST Experiment, planning and requests for 2013-2014

111th SPSC meeting

Giovanni Cantatore (University and INFN, Trieste)

for the

CAST COLLABORATION

CEA Saclay

CERN

Dogus University

Lawrence Livermore National Laboratory

Max-Planck-Institut for Solar System Research/Katlenberg-Lindau

Max-Planck-Institut für extraterrestrische Physik

Max-Planck-Institut für Physik

National Center for Scientific Research Demokritos

NTUA Athens

Institut Ruđer Bošković

Institute for Nuclear Research (Moscow)

TU Darmstadt

University of British Columbia

University of Chicago

Universität Frankfurt

University of Patras

University of Thessaloniki

Università di Trieste

Universidad de Zaragoza

CERN-SPSC-2013-027 / SPSC-SR-123
14/10/2013

1 Introduction

The CAST experiment has been taking data since 2003 providing the most restrictive experimental limits on the axion-photon coupling for a broad range of masses. The CAST experiment has covered axion masses up to 1.18 eV. During 2012 the magnet bores were filled with ^{4}He revisiting a narrow band of solar axions or ALPS rest masses. Analysis is in progress.

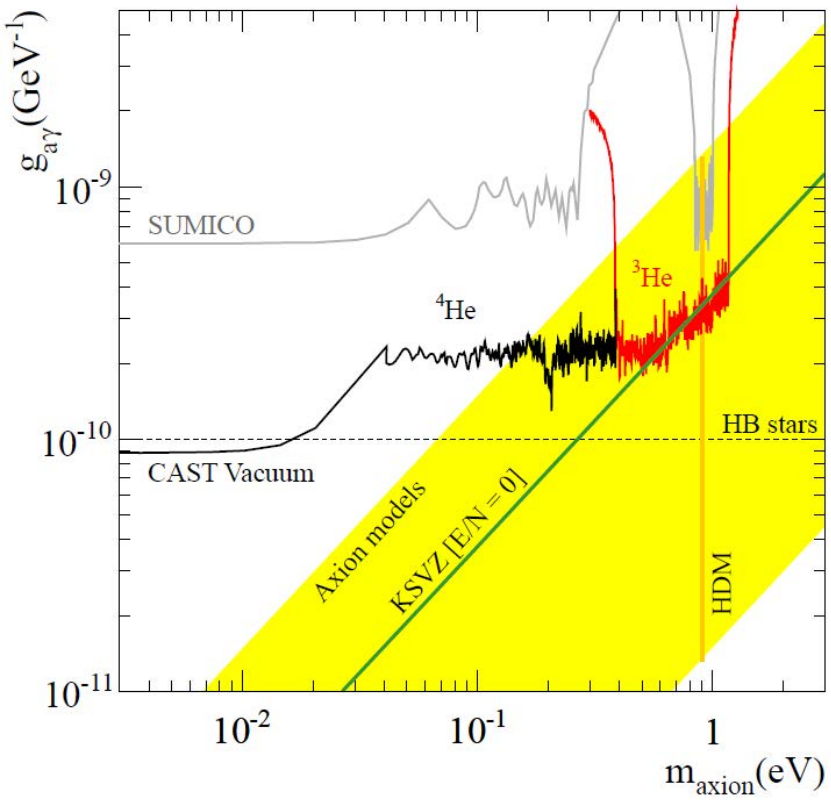

Figure 1 - Exclusion regions in the m_a–$g_{a\gamma\gamma}$ plane achieved by CAST running in the vacuum, with 4He, and 3He as buffer gases in the magnetic pipes. The maximum Helium gas pressure was 105mbar. The 3He results are in red. We also show constraints derived from Sumico, horizontal branch (HB) stars, and the hot dark matter (HDM) bound. The yellow band represents typical theoretical models, with the green solid line being the so-called KSVZ model for E = N = 0.

CAST has further improved the Micromegas background level, which allows to reach a still better sensitivity during our present data taking period with vacuum inside the magnet bores. In addition, new low-threshold detectors, i.e., the solid-state detector (SDD) being already operational, and the InGRID detector to be commissioned soon, transformed already CAST to the first solar chameleon helioscope. CAST is thus an experiment searching in the most mysterious sector of dark energy. In parallel, CAST is expanding its sensitivity also to particles like chameleons, even if they couple (only) to matter. This can be achieved with an in-house-made force sensor, which is a novel and highly interdisciplinary approach. This equipment is being tested and fine-tuned in the laboratory at a home institute. In addition, CAST has performed measurements with a PM in the visible, providing limits for the kinetic mixing coupling constant between photons and Hidden Sector photons.
Finally, CAST looks into the future aiming to eventually utilize the novel “dish antenna” concept introduced by people in DESY. A feasibility study is presently in progress, and

CAST has the potential to convert to a *tracking haloscope* of (streaming) relic axions, or, ALPS as they are advocated theoretically since some time [1],[2].
This report is organized as follows: in Section 2 we describe the activities in the experiment as well their present status while section 3 is devoted to proposals for 2014. Within Section 2 we report about the status of the system, the status of Micromegas detectors, the Ingrid detector, work on low threshold solid state detectors, CFD simulations, status of the analysis, paraphoton measurements, and sun filming. Subsections of Section 3 describe Micromegas detector upgrades and future plans, new planned optics, a proposed novel force sensor to measure the flux of solar chameleons, and the vacuum runs physics motivations both for solar WISP physics and for using CAST as a tracking haloscope for relics. The last part of the document contains the proposed schedule for 2014 and requests for CERN resources.

2 Status Report

2.1 Activities in CAST during Shutdown 2012-2013

At the end of the ^{4}He data taking, the SSMM detectors were dismounted to allow the XRT-CCD team to make a cold-magnet alignment check together with the CERN surveyors. This was to complement the previous check done with the magnet warm. The laser, aligned with the axis of the cold bore, was expanded to fill the entire bore and focused at infinity. The spot coordinates that were observed on the CCD detector 'live display' were 38-109 (pixels) in close agreement with the spot coordinates used for the analysis (35-108).

Following this, there was a period of tests on the magnet to improve the understanding of the gas dynamics and magnet temperature systematics using ^{4}He fillings of the cold bore. This led to the definition of additional temperature sensors to be installed in the 2012-2013 shutdown.

The magnet was force-warmed between 7-18th December and the isolation vacuum broken with dry air to atmospheric pressure on the 20th December to ensure the magnet was at room temperature by the start of 2013. Scaffolding was erected to allow access to the top of the MFB in order to change a severely leaking bellows valve on the cryogenic system. The repair eventually took 3 months as the new bellows had to be custom made.

In parallel, the vacuum systems at the MRB end of the cryostat were removed and the cryostat end plate removed by the start of February 2013 (Figure 2). Meanwhile the large cryostat bellow at the MFB end of the cryostat was opened. Before the intervention to remove all the fragile temperature instrumentation, a survey was made of the precise positions of all sensors in order to improve the precision of the CFD simulations.

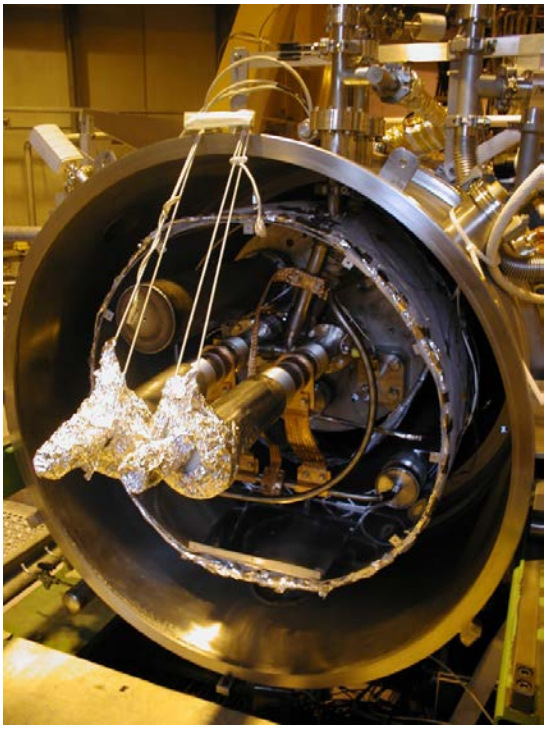

Figure 2 - MRB end of cryostat opened

In view of the on-going shutdown work, which immobilized the magnet, a sun filming run in late March was not possible.

Mechanical studies on the load-bearing properties of the MFB XRT platform were completed by engineers from EN-MME. They concluded that to add ~ 850 kg of new shielding onto the XRT platform required a strengthening of the welds on the steel support plate to which the XRT platform is bolted. TIG welding work was carried out by EN/MME in mid-April.

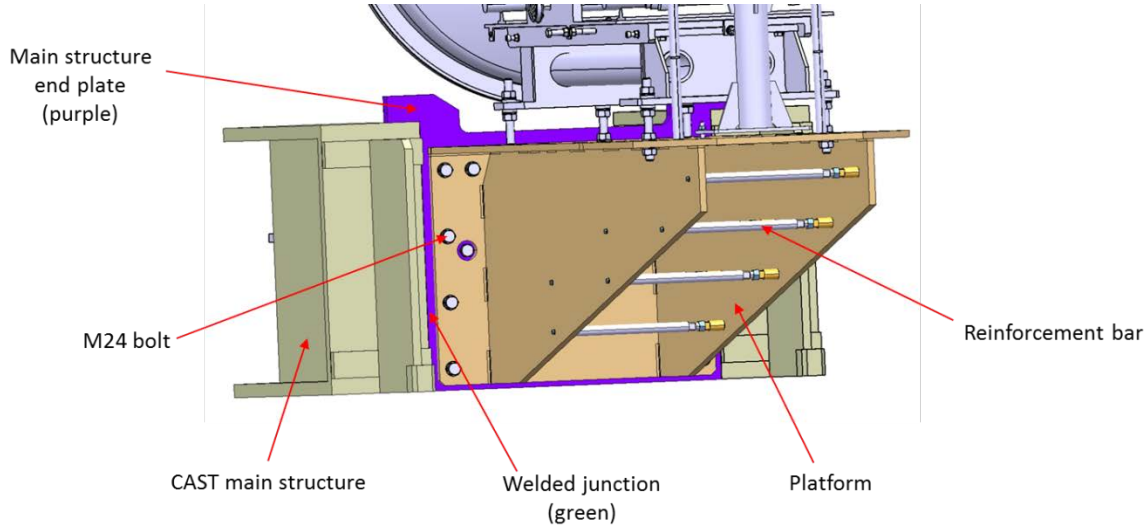

Figure 3 - Schematic of the fixation by bolts of the XRT platform to the CAST magnet main structure (green) via an endplate (purple) welded to the main structure

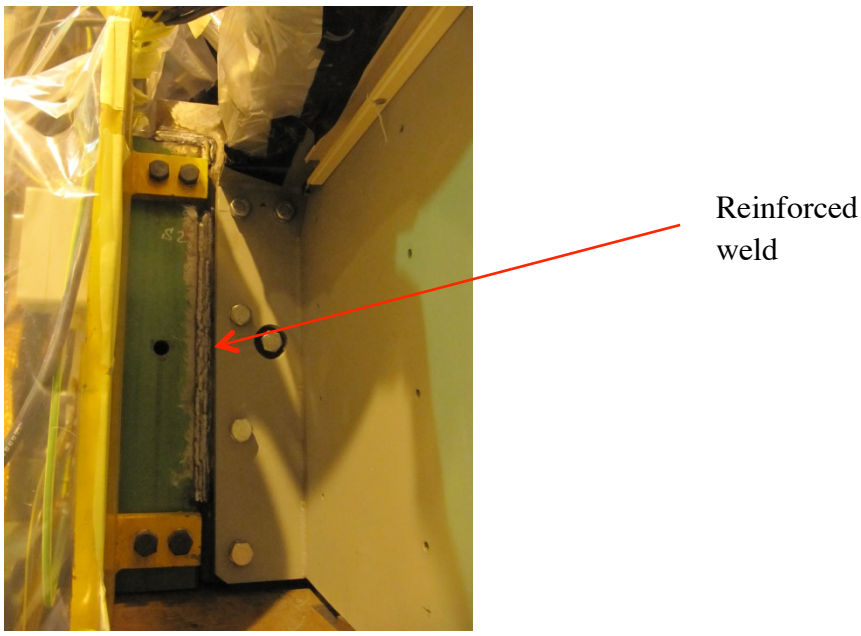

Figure 4 - Picture of the region of the welded junction after reinforcement

A survey was made before and after welding, which indicated that a small change in vertical angle of the platform (0.6 mrad) had occurred. The XRT, in any case, will be completely realigned when returning from re-calibration in PANTER.

Before closing the cryostat, the internal ^{3}He gas system pipework was completely decoupled from the cold bore vacuum circuit but left mechanically and thermally connected (for possible future use if a need arises). The four x-ray cold windows were removed and replaced by the original 'open flanges equipped with cross-wires for optical alignment of the XRT's (Figure 5).

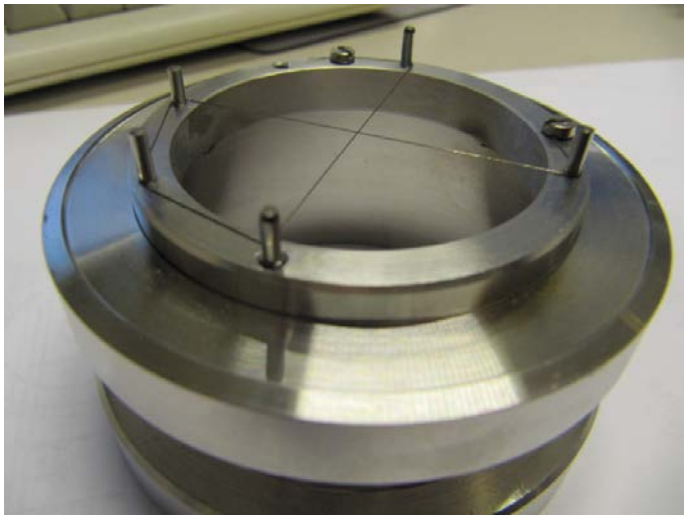

Figure 5 - Replacement windows with cross-wires.

On the MFB side of the magnet, the windows were coupled to the vacuum pipe extensions that run through the MFB tower. The vacuum joints were custom-made wedge shaped copper in order to improve the alignment of the vacuum line extensions to the cryostat end plate at the XRT platform.

Before closing the cryostat, a number of new temperature sensors were added to the magnet for further tests on the magnet temperature systematics. After internal leak tests, the cryostat was closed and pumped down. Leak tests revealed a small leak on a large cryostat flange, which was solved without having to reopen.

In parallel with the work on the cryostat, there were extensive maintenance and repairs on a troublesome main compressor of the CAST cryogenics system. This indeed determined the time scale for restarting CAST. After vibration tests of the compressor, the CAST cool-down started on 26 July 2013. The magnet was cold on the 8th August 2013.

Magnet temperature systematics tests were first carried out, tilting the magnet for different liquid ^{4}He coolant heights in the 1.8 K heat exchanger. In mid-August the magnet quench training took place. The magnet was powered for the first time for a test quench at 1500 A, the magnet then reached 12960 A before quenching, the next time the magnet reached 13050 A without quenching (operating current is 13000 A).

At the end of August the MPE-XRT was removed from the XRT platform ready for shipment to PANTER for re-calibration. The vacuum systems for the SSMM were then installed. At the start of September the Zaragoza team installed the SSMM detectors including a larger veto system.

Next, welding took place for the fixations to support the new shielding platforms for the SRMM and InGrid. The SRMM was then installed and after a mechanical safety report to the Safety Group, permission was granted to add the shielding for both the SRMM and the InGrid detectors. The counterweight under the XRT platform was reduced in order to compensate for the addition of load on the platform so as to maintain the same loading on all the magnet movement pivot points of CAST. Finally the small SDD was installed on the remaining beam line on the XRT platform.

With the full complement of detectors and shielding, a complete survey GRID was undertaken just prior to the September sun-filming period. Data taking started in parallel with the sun filming on the 22 September 2013.

2.2 Detector upgrades, status & performance

2.2.1 Micromegas upgrades

All Micromegas detectors are being read-out with new electronics in the 2013 CAST data taking campaign. These electronics were developed at CEA-Saclay for the Micromegas detectors of the T2K experiment, and have been used in different CAST test-bench setups. It is a fast and modular system that amplifies and digitizes the pulse signal of every strip (see Figure 6, left), generating more information than the previous one, based on the Gassiplex,

which only provided the integrated value of the signal for every strip. The basic component of the new electronics is a Front End Card (FEC), which contains 4 ASIC chips, each of which handles 72 physical channels. The signals from the Micromegas detector are fed to the electronics via flexible cables, allowing their placement tens of centimeters away from the detector chamber. This fact minimizes the potential contribution to the background level due to the radioactivity of electronic components.

In addition, dedicated measurements using PIXE (Particle Induced X-ray Emission) in the CAST Detector Laboratory at CERN have allowed calibrating the detectors at several x-ray energies (see Figure 6, right). These measurements provide a better characterization and understanding of the detector response as a function of the incident x-ray energy.

Both new electronics and dedicated tests will potentially allow an increase in the rejection power of the data analysis, and thus, an improvement of the background level of CAST Micromegas detectors.

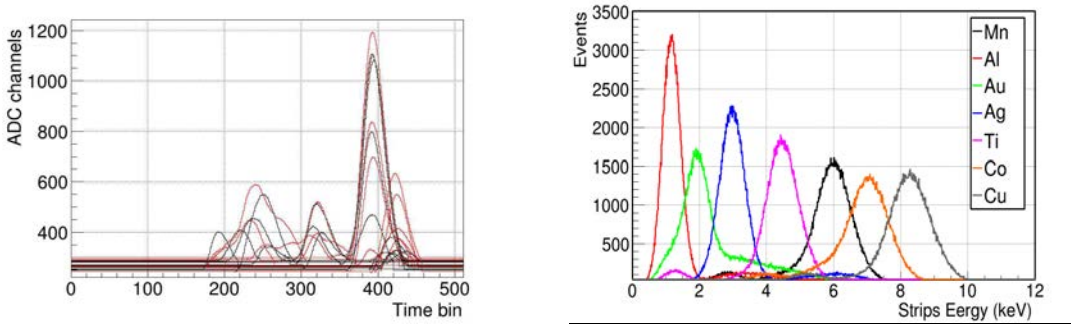

Figure 6 - Left: *x* (black) and *y* (red) strip pulses of CAST-M10 detector for a background event. Right: CAST-M18 energy spectra of some calibrations done with different target materials in the x-ray beam of the CAST detector laboratory.

2.2.2 Sunrise Micromegas

The Sunrise Micromegas (SRMM) detector has been redesigned. The upgrade is done basically at two levels: a) improvements in the shielding, following the Sunset detectors (SSMM) setup; and b) improvements of the gas chamber properties.

a) The changes that produced an improvement of approximately a factor 4 in the SSMM background level in 2012 have been extensively applied here. The new Sunrise Micromegas chamber is all made out of copper, including the *raquette* on which the detector is supported and which brings the signals and HVs out of the shielding. The lead shielding is the thickest possible (around 5 cm) given the mechanical constraints (see Figure 7, right). As in SSMM, the dirtiest components from the radiopurity point of view have been replaced by Polytetrafluoroethylene (PTFE) and copper, which are proven to be clean. Examples of the improvements are: the use of PTFE foils to avoid fluorescence; the reinforcement of inner copper shielding; the minimization of the signal extraction outlet and the enlargement of the lead external shielding; PTFE gaskets instead of Viton ones. The main differences with respect to the present SSMM is the future use of a smaller window, when the x-ray focusing device will be installed

(in the course of the 2014 data-taking) and the absence of a Plexiglas neck crossing the shielding. In this way, the two main weak points of the shielding will be minimized. Finally, as for the new SSMM, a cosmic veto, especially designed for the SRMM, will be installed in 2014.

b) The gas chamber, Faraday Cage and inner shielding are completely integrated in the new SRMM design. The Plexiglas base (*raquette*) has been replaced by a copper one, which is the base of the shielding. All the high voltage connections, including the cathode one, are implemented in the detector printed board. Like this, the connections with the power supply and electronics, which are potential radioactivity sources, are moved away from the detector body, without the need for exit points in the shielding. A new field shaper has been designed, printed on a flexible multilayer circuit with Polyimide as substrate. The circuit contains two tracks, 10 mm thick each, to emulate the typical conductor rings. The outer side of the circuit is used to bring the HV connections from the detector board to the field-shaper tracks and the drift cathode (see Figure 7, left). An inner PTFE foil prevents fluorescence from these tracks without disturbing the field lines (see Figure 8). The detector board has been redesigned to include the new HV connections.

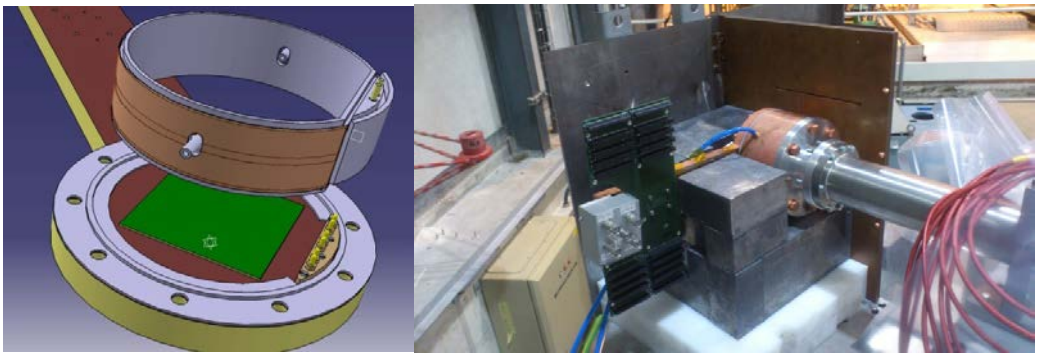

Figure 7 - Left: schematic view of the new SR Micromegas detector design. The readout (green) and the HV connectors (yellow pins) are driven through the *raquette* to the electronics. The field shaper (brown) made out of two printed copper strips on a polyimide flexible circuit. Right: SR Micromegas detector partially shielded installed in the line.

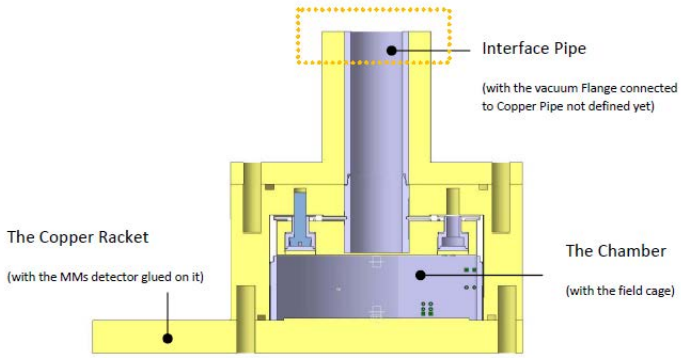

Figure 8 - Cross-section of the detector, chamber, inner shielding and interface to cold-bore.

The new Micromegas detectors have been designed in such a way so as to be mounted on any magnet bore, be it SR or SS, in view of future detector replacements.

2.2.3 Sunset Micromegas

In the 2012 upgrade of the Sunset Micromegas, a preliminary scintillator veto with ~44% geometrical efficiency for cosmic muons was installed. It produced a reduction of 25% in the background level. The contribution of cosmic muons to background and its possible mitigation by means of higher efficient vetos has been evaluated in dedicated experimental setups. It was found that further reductions in background level were possible, therefore a higher-efficiency system based on two plastic scintillators was designed, manufactured and installed (see Figure 9, left). This installation required some changes in the allocation of the vacuum elements of the Sunset line. The computed geometrical efficiency (without including production of secondary particles or quantum efficiency) of the system is higher than 90%. A preliminary analysis of the first ~300 hours of the 2013 SS1 data with this setup shows that, keeping the same signal efficiency as for the 2012 data, the background level has been reduced from $\boldsymbol{(1.29 \pm 0.05)x10^{-6}\ keV^{-1}\cdot cm^{-2}\cdot s^{-1}}$ to $\boldsymbol{(6.2 \pm 0.9)x10^{-7}\ keV^{-1}\cdot cm^{-2}\cdot s^{-1}}$ in the CAST energy Region of Interest (RoI) (see Figure 9, right). The background level is for the first time below ~10^{-6} $keV^{-1}\cdot cm^{-2}\cdot s^{-1}$, a milestone in the Micromegas ultra-low background program. The reduction in the background level matches the expectations presented in previous reports, representing a factor 2 of improvement in Sunset Micromegas background level with respect to 2012. Two years of intense upgrades are summarized in nearly one order of magnitude of improvement in background level. The causes of the improvement are shared between the electronics and cosmic veto upgrades.

It is noticeable that this level has been obtained even if the installed drift cathode is made out of aluminum (instead of more radiopure copper ones due to technical difficulties). The contribution to background of the aluminum cathode was evaluated in a dedicated setup in the Canfranc Underground Laboratory (LSC), and was assessed at ~$5x10^{-7}$ $keV^{-1}\cdot cm^{-2}\cdot s^{-1}$. The replacement of this cathode by a copper one will very likely provide an additional improvement that will allow reaching or even surpassing the current best background level achieved by a Micromegas detector underground (~10^{-7} $keV^{-1}\cdot cm^{-2}\cdot s^{-1}$, equipped with Gassiplex electronics).

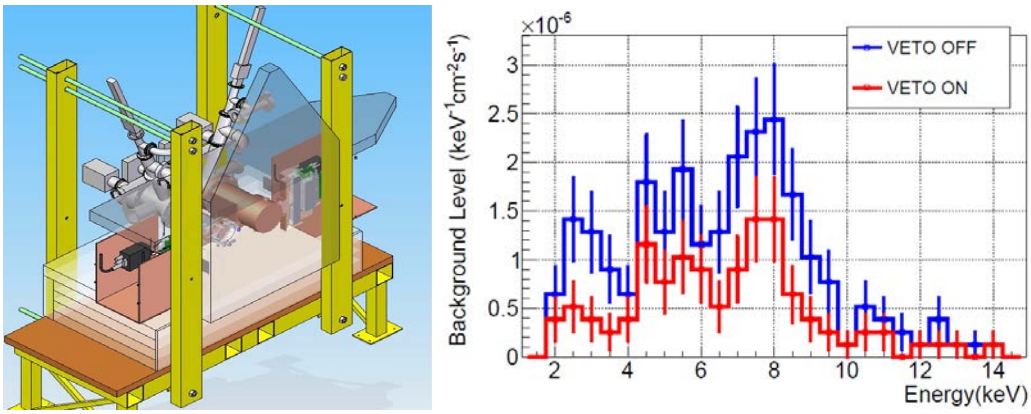

Figure 9 - Left: schematic view of the new scintillator cosmic vetos in the sunset line. Right: Background energy spectra of the Sunset 1 detector from a quick-look analysis of 2013 data.

2.2.4 InGrid

InGrid detectors are made of a pixel readout ASIC (Timepix) and an integrated mesh which is applied with post processing techniques on the chip. The hole structure of the grid is adapted to the 55 μm pitch of the pixels and well aligned with them. This setup allows the detection of single primary electrons already at a moderate gas amplification of ~5000 and with a high efficiency (>90%). The precise position of the primary electrons can be used to suppress background events of charged particles creating long tracks. An additional advantage of this new detector is its low detection threshold. At sufficiently high gas gains the threshold level can be adjusted, so that no noise hits can be observed, but high detection efficiency can be retained. Therefore, photons with energies so low that they release only 1 electron from the gas can be detected theoretically. In practice a larger number of primary electrons will be necessary to identify the photons.

A detector based on the MM detectors has been built to fit behind the XRT. The small focus point of the telescope can be covered with a single InGrid detector and an excellent background reduction is expected. In 2013 three major tasks were addressed to prepare the operation of an InGrid-based detector in CAST.

2.2.4.1 Detector test in the CAST detector lab

In April this year the InGrid detector was mounted on the X-ray tube in the CAST detector lab and the detector response to X-ray photons of different energies was tested.

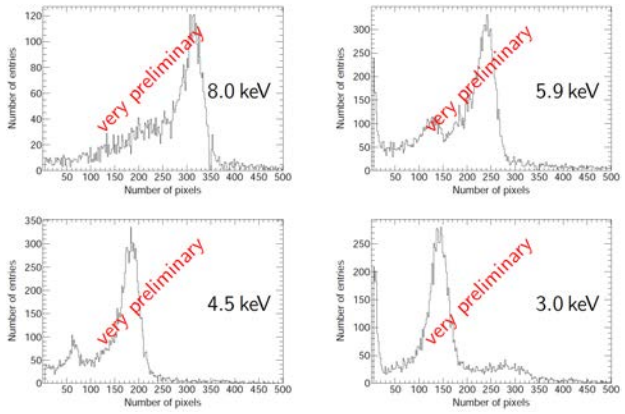

Figure 10 - Number of pixels in events with photons of various energies converted.

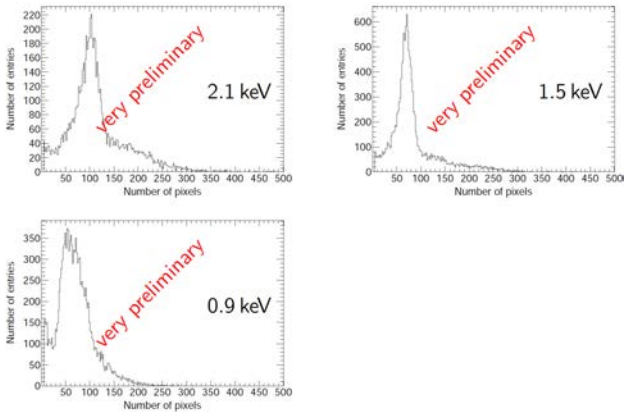

Figure 11 - Number of pixels in events with photons of three lower energies converted.

Figure 10 and Figure 11 show the energy spectra of various photon energies. The energy is given in primary electrons, which has to be multiplied by the average energy per ion pair in this gas (~25 eV). The detector could be tested with photon energies down to 900 eV. Because of the tight vacuum constraints of the X-ray tube a differential pumping scheme was necessary. The first of the two windows was a 4 μm polypropylene foil, the second window corresponding to the cathode of the detector consisted of a 2 μm Mylar foil with a 40 nm coverage of aluminum. Because of the high absorption at low energies, a large fraction of the 500 eV photons were absorbed, and no useful measurement could be done. However, a few photons were observed proving, that the detector is sensitive, if the photons can enter.

Several shortcomings of the detector had been observed during the measurements and have been addressed for the final design of the detector: The thick first window will be replaced by a thinner 0.9 μm mylar foil to improve the sensitivity to low energetic photons. A significant amount of random hits were observed which are UV photons either passing through the transparent detector walls or originating from discharges of the cathode and passing through the cathode. Therefore, the detector will be covered with black tape. Finally discharges from the cathode into the vacuum were observed, which will be prevented in CAST by covering the open metallic parts of the cathode with an insulating varnish and by improving the geometrical layout of the mylar foil strongback. The pitch of the strongback bars has been reduced decreasing the force and thus the leakage rate of the gas into the vacuum.

2.2.4.2 Development of a new experimental line for the sun rise position VT4

The InGrid detector will replace the CCD-detector next year. For this the connection between detector and XRT has to be redone. The CCD detector could be placed and operated in the high vacuum of the XRT, but the InGrid detector is filled with 1 atm of Ar:iC_4H_{10} 97.7:2.3. To reach the XRT vacuum level of 10^{-7} mbar a differential pumping system has to be developed. Based on the experience from the MM detectors such a system has been designed and all relevant parts have been purchased or machined. The parts will be assembled and the correct functionality of all parts will be tested at Bonn before installation at CAST. The beam line has been designed, so that the detector is still movable and the InGrid can be aligned with the focus point of the XRT. The alignment will be experimentally verified by measurements with a pyro-electric X-ray source on the sunset side.

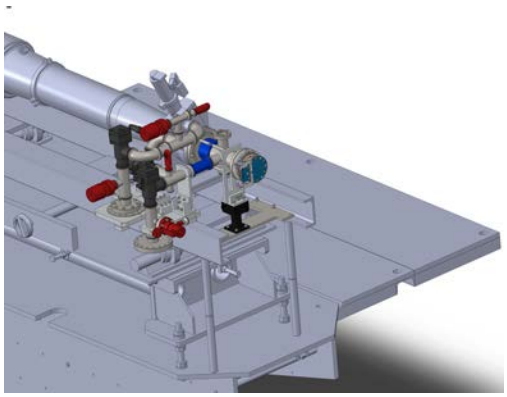

Figure 12 - Components of the differential pumping setup.

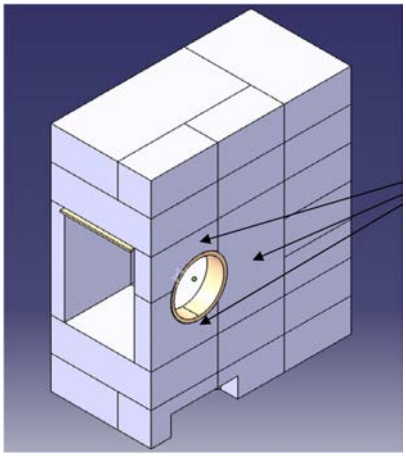

Figure 13 - Lead shielding of InGrid detector.

To shield the detector against external radiation like cosmic rays or radioactive decay products a lead shielding was designed at the University of Zaragoza. It covers the detector with 10 cm of lead on the sides, 10 cm on the top, 2.5 cm at the front and 2 cm to the back, where the wall of the SR8 does not permit a thicker layer.

2.2.4.3 Improvement of the analysis

In the previous analysis, distributions of various events shape variables were used to define a likelihood ratio and distinguish photon-like events from track-like events. In a new study several different algorithms implemented in TMVA/ROOT such as neural networks and boosted decision trees were investigated to replace the likelihood ratio. Distributions of 25 parameters were used to train the algorithms to separate photons from tracks. Indeed, several algorithms showed a better performance and will be used in the next data analysis to estimate systematic errors. Figure 14 and Figure 15 show the background rejection in dependence on the signal efficiency, if the complete 55Fe spectrum was used for the training procedure (Figure 14) and if only events with energy between 5.6 and 6 keV were used.

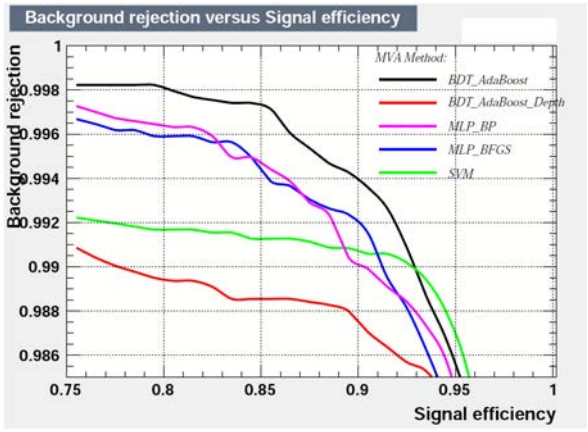

Figure 14 - Background rejection in dependence on the signal efficiency, if the training was done with the complete 55Fe spectrum.

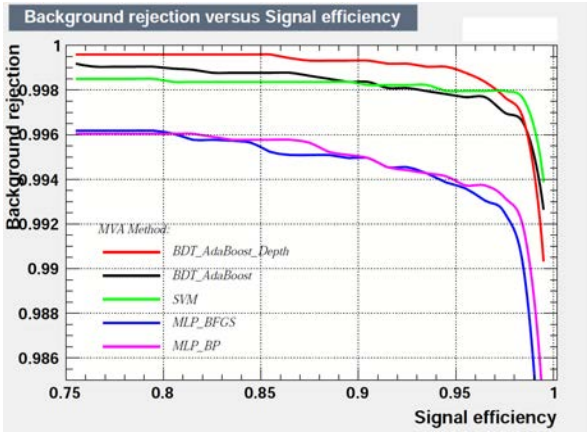

Figure 15 - Background rejection in dependence on the signal efficiency, if the training was done only the photons of the energy 5.5-6.0 keV

To investigate the performance of all analysis steps for low energetic photons, a set of artificial 1 keV photons was created by using events of the ^{55}Fe-photoline and removing hits randomly chosen, so that the remaining number of photons corresponds to the expected for 1 keV photons. Figure 16 shows an original event on the left side and the mockup 1 keV event on the right side.

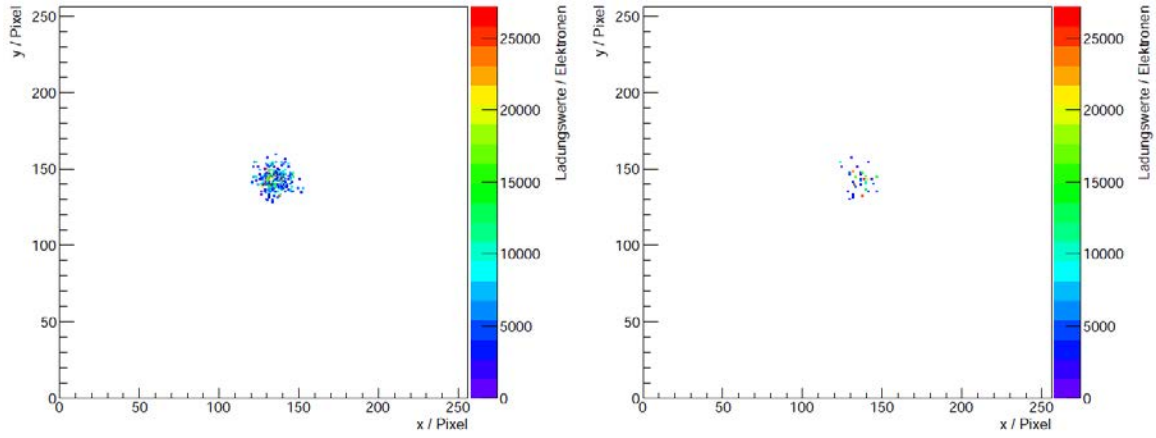

Figure 16 -55Fe event (a) and same event with ~80 % electrons removed (b).

With these events the efficiency of the background separation of 1 keV photons was studied. At first the signal efficiency of 1 keV and similarly produced events of 0.5 – 2 keV photons was studied, when the algorithm was trained with photons of 5.9 keV (see Figure 17). Then the separation of 1 keV photons from the background was studied, when the algorithm was trained with mockup 1 keV photons (see Figure 18).

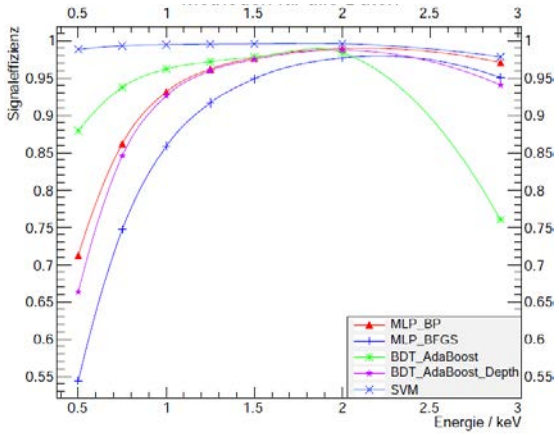

Figure 17 - Signal efficiency of low energetic photon events, when the algorithm is trained with 5.9 keV photon events.

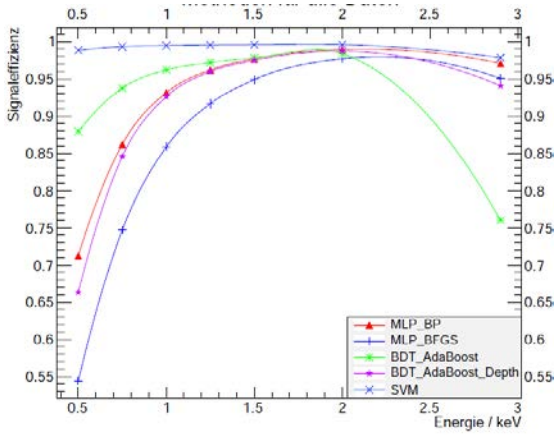

Figure 18 - Background rejection versus signal efficiency of 1 keV mock-up photons, when the algorithms are trained with 1 keV mock-up photons.

2.2.4.4 Work on the x-ray telescope line

In preparation for the new experimental campaign, we have removed the x-ray CCD detector. It will be replaced by the new InGrid detector developed in Bonn, which extends the x-ray sensitivity to low energies (below 1 keV), enabling us to search for low-energy axions and other particles like chameleons. The x-ray CCD has been removed from the setup in June 2013 and is now packaged and ready for shipment back to the Max-Planck Institute for Extraterrestrial Physics (MPE) in Garching. The preliminary 2009 CCD data analysis is finished. The complete treatment of all 3He data will be done by the end of 2013.

In addition to the CCD detector, we have also removed the x-ray telescope to send it for inspection at the MPE in Garching. To ensure that the x-ray reflectivity of the telescope has not degraded significantly since the last tests in 2009, the reflectivity of the x-ray optics will be tested at the PANTER x-ray facility, which is a dedicated test facility for x-ray optics. Unfortunately, PANTER is currently used to capacity for testing equipment of the upcoming eROSITA space mission, so our x-ray telescope cannot be tested before November 2013. The x-ray telescope has been removed from the CAST setup in August. It has been packaged and will be transported to PANTER in the upcoming weeks. The measurements at PANTER will take 1-2 weeks and the telescope will be transported back to CAST at the end of 2013, so that it can be installed back into the setup at the beginning of 2014. Once the x-ray telescope has been installed and re-aligned to the magnet bore, the InGrid detector will be integrated into the existing infrastructure and control systems (for example vacuum controls and data acquisition). While this will require considerable work, the measurements in 2014 are not expected to start before May, so there will be sufficient time to complete the installation and thoroughly test the whole setup with the new detector before the start of the new measurements.

Figure 19 - MPE X-ray telescope being removed from the CAST beam-line.

2.2.5 Low Energy Searches

2.2.5.1 Silicon Drift Detector (SDD) on CAST

Small SDD

In view of the availability of the MPE-XRT beam line for several months this autumn whilst the XRT is recalibrated, a low-energy threshold detector was chosen to occupy the beam line for a first look in a low energy range now accessible in the Vacuum run. The most well understood low energy detector available to us was a small area detector used in the CAST x-ray lab. The detector has a good resolution at low energy (65 eV at 500eV) but does not have any imaging capabilities. The detector has already been mounted on CAST for several days during the shutdown and no serious noise pickup problems were observed during magnet movement tests.

The AMPTEK XR-100CR Silicon Drift Detector (SDD) has been used as a reference detector in the CAST X-ray lab at CERN for the last year. It is combined with a PX5 Digital Pulse Processor and an applications program, which allows remote control of many detector parameters (operating temperature, high voltage, threshold, preamplifier gain etc.). The normal operation of the system is as a multi-channel analyser. In order to operate on CAST, it was necessary to modify the operation of the PX5 to provide to the PC the event list including timestamp and energy channel for each event above threshold.

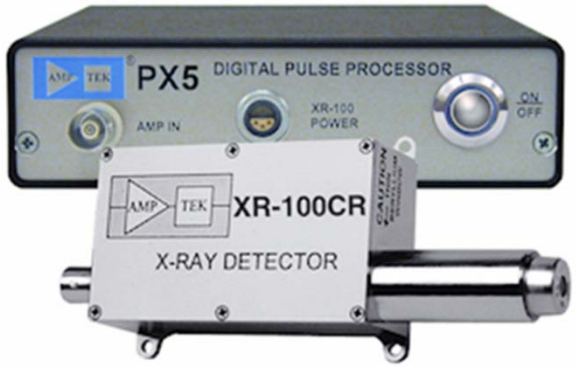

Figure 20 - SDD & PX5 from AMPTEK (see text).

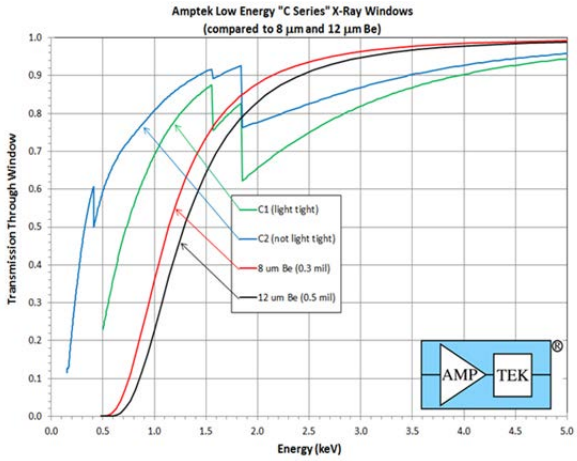

Figure 21 - Performance of the C2 window.

The SDD detector operates in a static vacuum at around 220K behind a small C2 window (16 mm^2) with X-ray transmission down to at least 200 eV as shown in Figure 21. The quantum efficiency of the silicon is not optimised for the very low energies since it was originally designed for operation behind a thick Be window. Combining the performance of the C2 window and the SDD silicon QE (from Amptek information) results in the response curves shown in Figure 22.

The minimum operating threshold in the laboratory is 150eV and the thermal noise tail extends beyond that threshold by an amount, which depends on the detector temperature. In order to operate the detector at 217 K and achieve the best noise levels, it is necessary to cool the SDD electronics box. This is achieved by connecting the electronics box to a copper block containing 6 mm diameter holes in which heat pipes are inserted. The other ends of the

heat pipes are inserted into a Peltier cooling device regulated to maintain 20 ˚C at the electronics box.

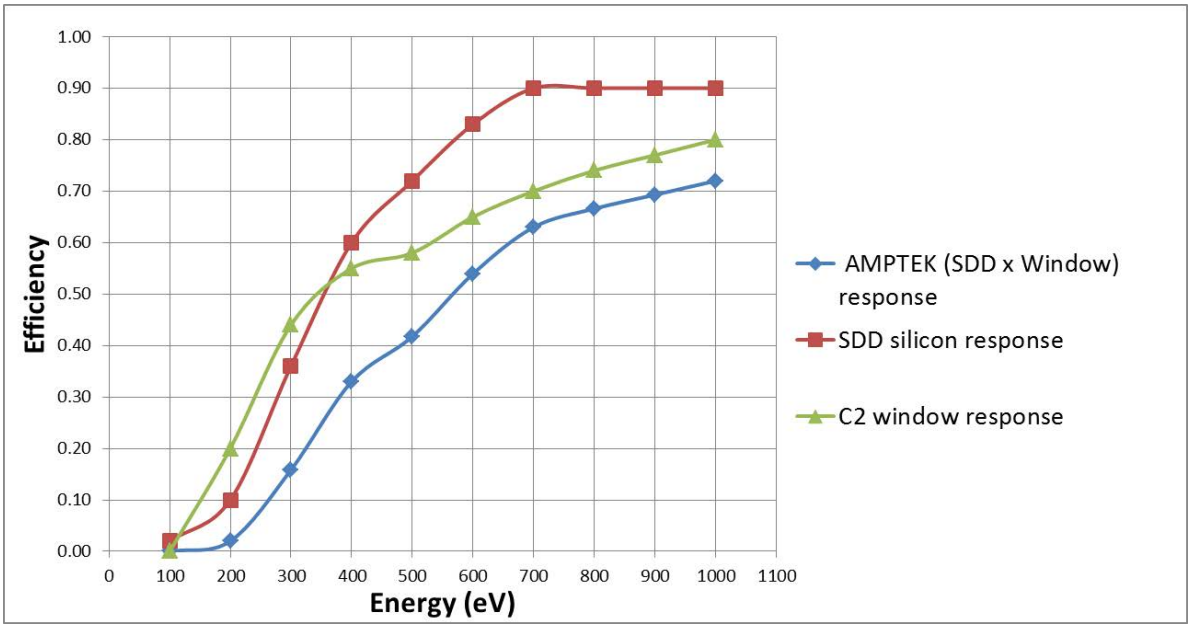

Figure 22 - Summary of SDD advertised performance figures.

A study of noise levels at low energies was carried out in the X-ray test lab. On the laboratory bench in air (but light tight) the noise spectrum at 220 K is shown in Figure 23 (at left). In Figure 23 at right, the detector is placed in the interior of a 12.5 cm thick lead box with the detector temperature of 217 K.

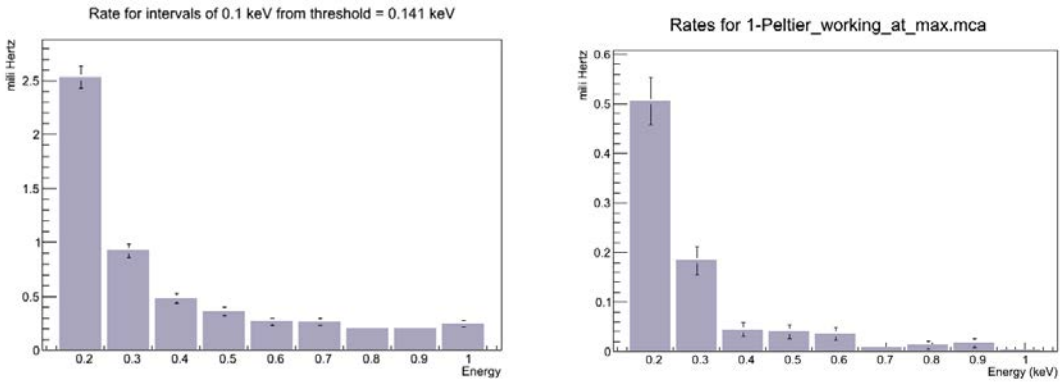

Figure 23 - No shielding 220 K (left), 12.5cm shielding + cooling detector at 216 K (right). See text.

Levels around $2x10^{-5}$/100eV/s above 350 eV were measured for the shielded case indicating a component of the background comes from Compton scattering of gammas. Mounted on CAST, the electrical noise rates will be higher than in the laboratory and may dominate the thermal noise at low energies. The thermal noise and Compton background will be minimised by cooling the detector electronics box to operate the SDD near to 216 K and install the maximum amount of shielding the geometry of the vacuum line allows. It will not be possible to have a complete shielding as in the lab.

The SDD and vacuum system were installed in the zone on the VT4 vacuum port of CAST at the start of September. In the following weeks the electrical and cooling systems were added

and optimised to minimise the electrical background noise, particularly from magnet movement motors.

The noise rate of the detector installed on the experiment, with magnet stationary, was similar to the laboratory unshielded rates. A possible source of noise was found to be from electrical impulses in the regulation system of the Peltier cooler which can be transmitted to the SDD by the heat pipes. After a period of 6 days running, the Peltier was switched off for 6 days to provide a comparison (the SDD temperature rose from 217 to 221 K). After this period, an intervention was made to install lead shielding and add a sheet of 0.5 mm thick AlN to insulate electrically but not thermally the SDD electronics from the copper cooling block in which the heat pipes were inserted. The SDD is now running at 217 K with lower background than the previous two periods of running.

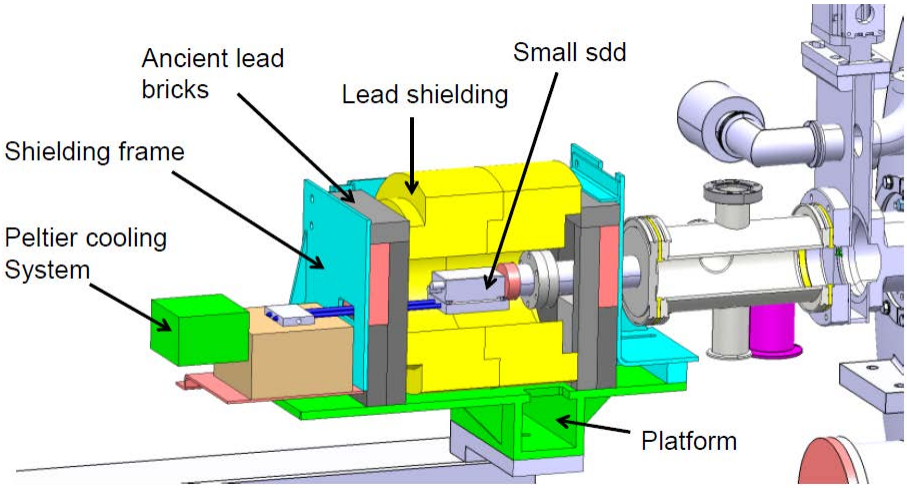

Figure 24 - Present setup at CAST for small SDD detector.

The layout of the detector system is shown in Figure 24. A photograph of the small SDD on CAST with half the shielding installed is shown in Figure 25.

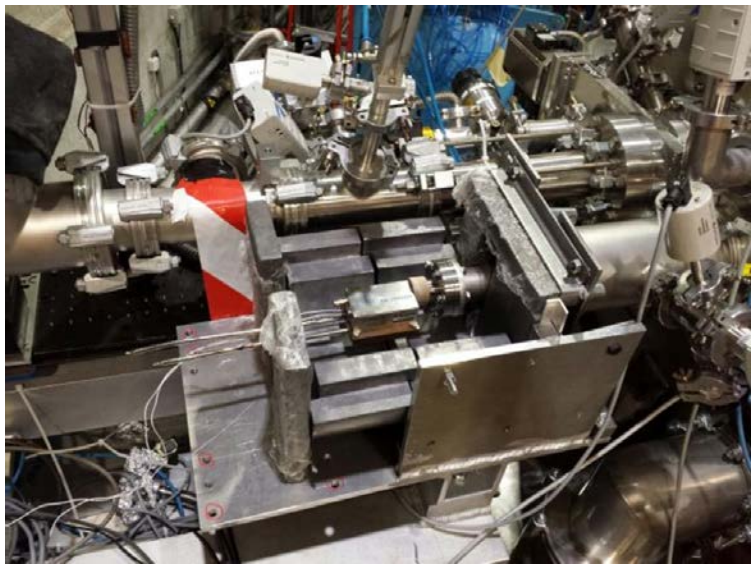

Figure 25 - The SDD installed in CAST together with half the shielding.

Whilst in the laboratory the SDD gain was very stable, the response of the SDD has been checked on CAST by using the low-rate 'x-ray finger' source located at the opposite end of the cold bore in the SSMM vacuum system. Figure 26 below shows a calibration spectrum produced from an 8h exposure to the x-ray generator with a pyro-electric crystal (AMPTEK-COOL-X) operating at 12 m from the SDD at the opposite end of the cold bore. The source was previously used together with the XRT/CCD system.

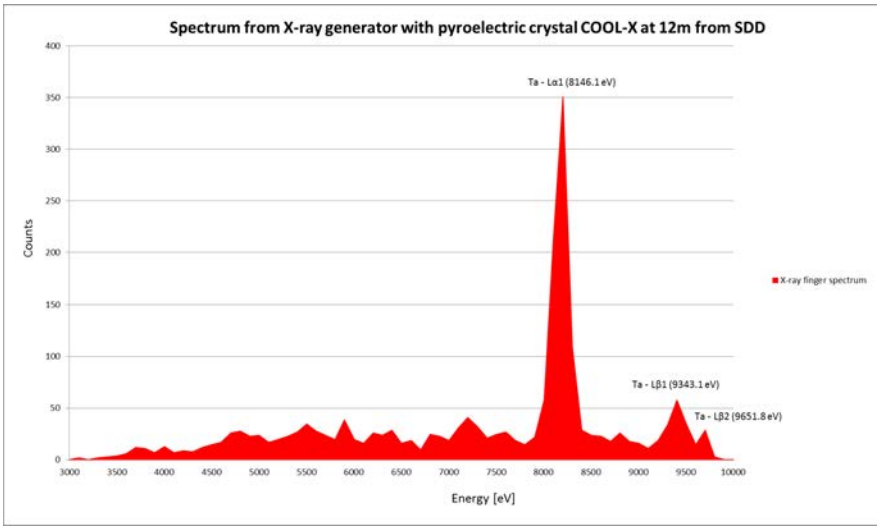

Figure 26 - Spectrum from an x-ray generator with a pyro-electric crystal (AMPTEK- COOL-X) situated at 12 m from the SDD.

The most recent tracking data with the SDD shielded and operating at 217 K has been analysed together with background data taken each night (field on, magnet stationary). A very preliminary comparison in the rates (per 76 eV per second) is shown in Figure 27. The plot comprises of 7 solar trackings totalling 10.3 hours and 36 hours of background data.

Considering the response curves of the SDD together with the thermal noise spectrum and the resolution (65 eV at 500 eV); only data with energies above 400 eV will be considered until a detailed study of the systematics in the region 140-400 eV is made.

The background rate above 400 eV in the SDD is well below 10^{-4} cts/100eV/s and similar to the shielded rates observed in the lab (Figure 23 at right) where there was a more complete shielding and a larger thickness of lead (12.5 cm compared to 6cm in CAST).

The planning for the SDD is to continue data taking in present conditions until the larger SDD is ready to be installed. This is estimated to be near the start of November 2013.

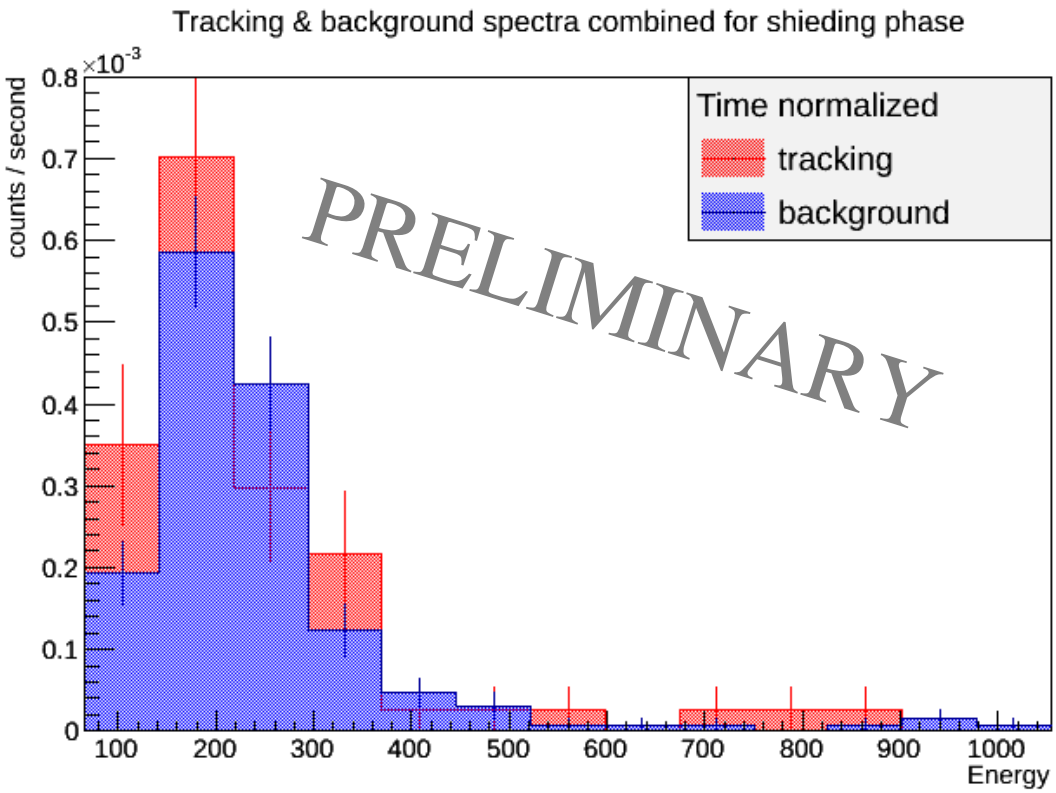

Figure 27 - Normalised comparison of tracking and background runs small SDD.

Large SDD

A larger SDD from PNDetector Munich is being prepared to replace the AMPTEK SDD on CAST. The new SDD will have an area 100 mm^2, six times the area of the small SDD and with a higher quantum response at low energies due to having no vacuum window and an optimised low energy response of the silicon entrance 'window' of the SDD.

A comparison of the quoted response of the PNDetector SDD compared with the AMPTEK SDD is shown in Figure 28.

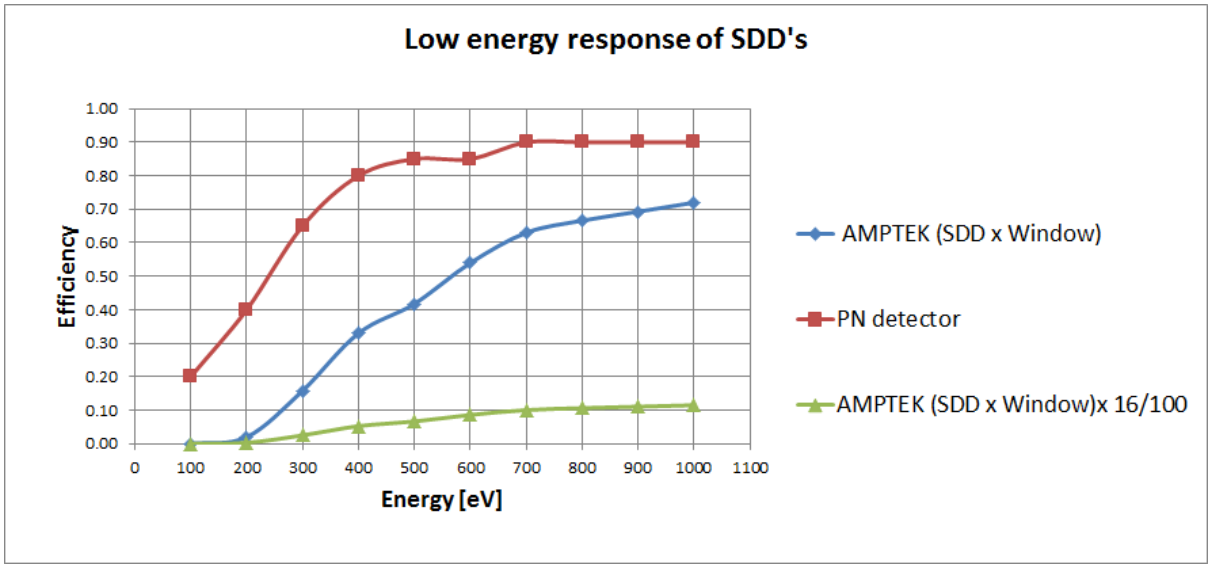

Figure 28 - Comparison of PNDetector with AMPTEK SDD response. The green curve also considers the relative areas of the two detectors (100 mm^2 and 16 mm^2 respectively).

Status of the large SDD: the vacuum system, shielding system and power supplies and cabling are now prepared. A dedicated PX5 is available for data acquisition of this device but has not yet been tested with the detector.

The large SDD will be mounted inside the vacuum on a copper plate, which also serves to hold the preamp card (Figure 29). A total of 5W of heat must be removed during operation to enable the SDD to operate at -30 ˚C.

The heat removal can be done passively with a 5° C temperature difference along the copper plate between detector and vacuum flange. The copper plate also contains two drilled holes in which heat pipes can be inserted to increase the cooling power so as to maintain the detector at an optimum -30 ˚C even if the detector is inside the shielding.

The cooling system will be upgraded by replacing the old cooling regulator with a more sophisticated computer-controlled regulator to reduce any noise pickup. The vacuum, noise and x-ray calibration tests of the whole system will be done on the CAST x-ray beam line starting on the 21st of October.

The planned layout for the large SDD is shown schematically in Figure 30, the present and future SDDs share shielding, cooling and PX5.

The planning for the large SDD is to test on the X-ray beam line for 2 weeks for energy calibration, preamp and grounding optimisation. When the performance is acceptable, it will be installed instead of the small SDD in approx. week 45. There will then remain about 1 month of data taking until the end of the 2013 run.

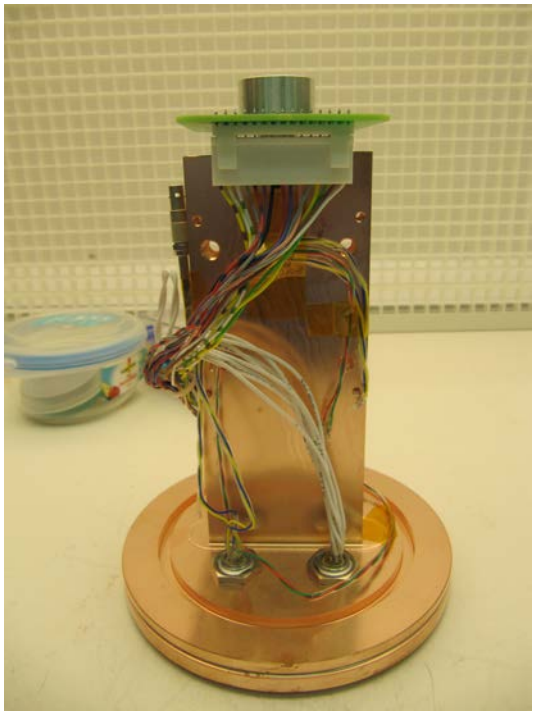

Figure 29 - Large SDD mounted on copper plate, which acts also as the preamp holder and heat sink for the detector.

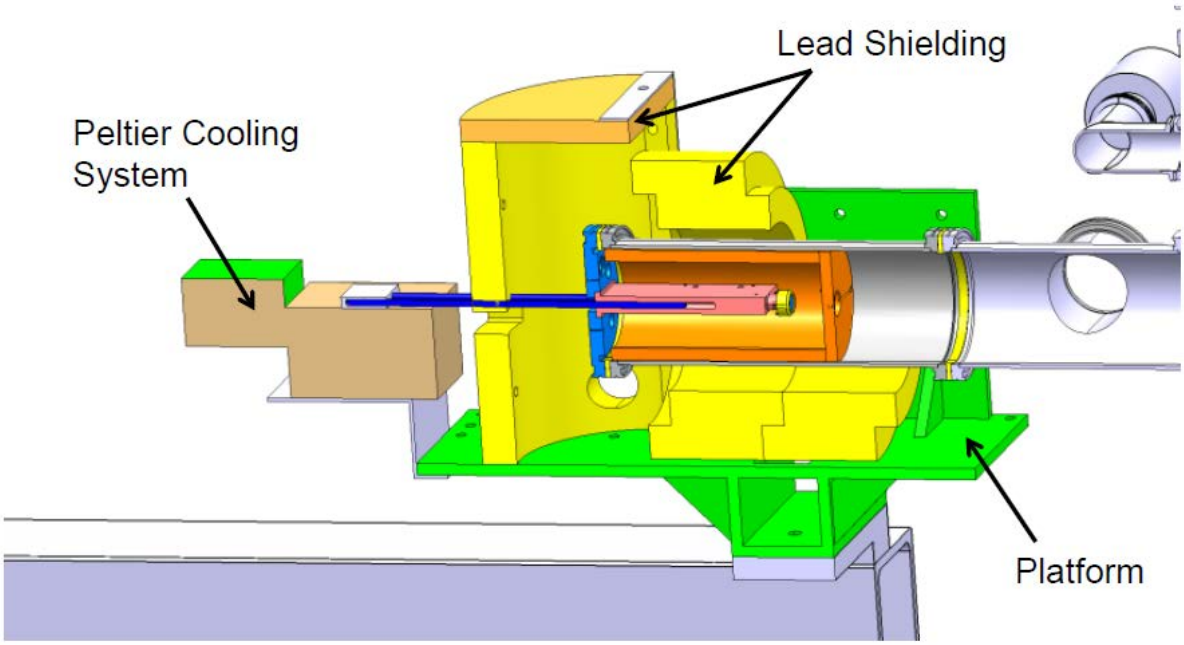

Figure 30 - Schematic layout of SDD on CAST

2.2.5.2 BaRBE

The light collection optics for the BaRBE low energy detection system have been removed from the previous location, in front of the Sunrise Micromegas detector, in order to free space for the new X-Ray Telescope being built at LLNL. The BaRBE optics will be redesigned and moved to a position in front of the InGrid detector where it can also exploit the focusing properties of the existing MPE X-Ray Telescope (see Figure 31). Since the expected beam diameter in the new BaRBE position is 16 mm, the mirror dimensions can be reduced down to the standard 25.4 mm (1") diameter optics ensuring the possibility of fitting the pieces through the available 40 mm diameter vacuum port. To avoid interference with InGrid, the mirror will be mounted on a motorized foldable mount based on a compact lever movement. The mechanical parts are being designed and manufactured in the INFN Trieste machine shop. Light will be extracted, as in the previous BaRBE optical system, through a matching lens and optical fiber up to an optical switch alternating between two outputs. A single detector can then look alternatively either at the beam or at the background, while two detectors can share beam time. The former scheme has already been implemented in the past[3] using a photomultiplier tube (PMT, instrument provided by Y. Semertzidis and D. Lazarus, BNL) as the single detector (see below for results on paraphotons obtained with this setup), while the latter will be tested with the new BaRBE setup, keeping the PMT as the "benchmark" detector and using a cooled Avalanche PhotoDiode (APD) as the second detector.

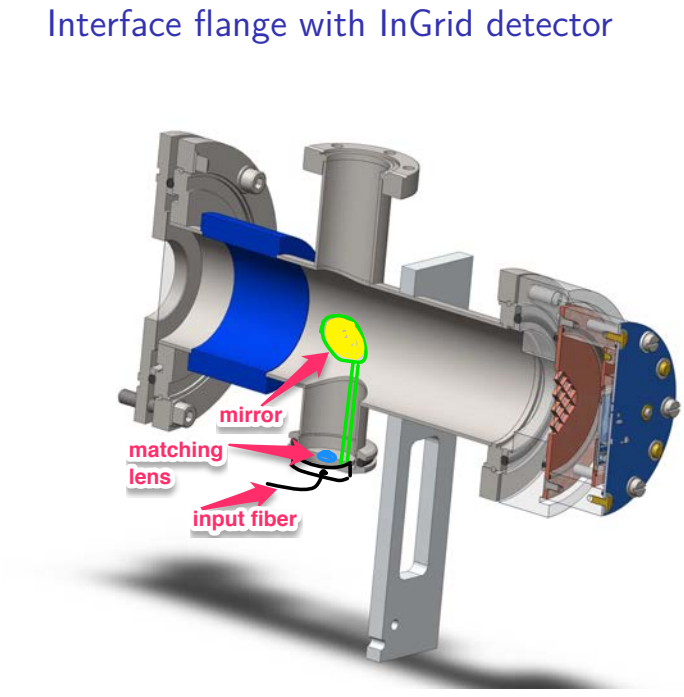

Figure 31 - Schematic drawing of the new BaRBE optics location on the interface flange of the InGrid detector.

2.3 Status of CFD simulations

The computational fluid dynamics (CFD) simulations are carried out in collaboration with the CFD team of EN/CV; significant progress has been made in the last year. The main aim of the simulations is to achieve a detailed understanding of the density distribution of the 3He gas in the magnet bores. The density profile plays an important role on the CAST analysis, since the axion-to-photon conversion probability depends strictly on the coherence length. The axion mass that CAST is sensitive to depends on the central gas density in the magnet cold bores.

The gas density in the cold bores cannot be measured directly; the only experimental measurements available are the number of moles of 3He gas inserted into the cold bores, the magnet temperature, the temperatures of the flanges and pipework near the extremity of the cold bores (on the X-ray cold window flanges and link volumes) and the gas pressure measured at one end of the cold bores in the link volume.

The measured cold bore pressure value with magnet horizontal varies as the magnet tilts during solar tracking. This variation while tilting is caused by the changing hydrostatic pressure of the gas column, a tilt-induced slow characteristic temperature transient in the magnet cryo-circuit and also due to the changing gas dynamics in the end-regions of the cold bores. For example at 83 mbar, the pressure rises by 1.05 mbar when moving from 0 to -6 degrees tilt angle.

Reproducing this strong pressure trend observed during tilting is a key indication that the CFD model reproduces the CAST conditions in a realistic way. Another, less sensitive, measure of the success of the model is to compare experimental and simulated temperature changes of the cold window flanges, which are affected by changing gas dynamics on tilting.

The extreme conditions in the 3He gas in CAST compared with the typical regimes that the CFD models have been developed for are a very challenging application for CFD (it is quite possible that no CFD turbulence model currently available will exactly simulate CAST conditions).

Simulations were made for a number of pressure settings in the CAST pressure range scan at a series of tilting angles, imposing turbulent or laminar flow solutions in the whole system and latterly, imposing turbulent or laminar solutions in different regions of the same cold bore. It was observed that the density distribution may vary significantly depending on the model chosen (as shown in Figure 32).

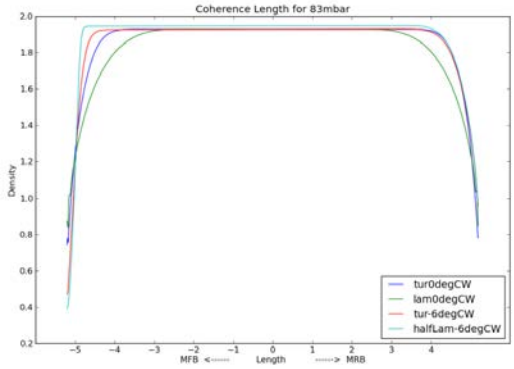

Figure 32 - Comparison of density profile for different models for horizontal and tilted simulations for 83 mbar.

After a thorough analysis of the results of the many different simulations, for the horizontal case: the laminar flow model was chosen for unheated cold windows (high densities of gas inside the cold bore, with windows ~ 12 K) and the turbulent flow model for heated windows (lower densities of gas, with windows maintained at typically 70 K). For tilted simulations, a half-laminar model was chosen, which is a composite description of the system with a turbulent solution in the lower one half of the cold bore smoothly joined to a laminar solution in the upper half. The temperature difference between the relatively warm cold windows and the 1.8 K cold bore created greater natural convection due to gravity in the bottom part and so turbulent flow is a more natural choice, while the upper part of the cold bore was set to laminar flow since stratification is likely to occur.

Figure 33 shows the pressure variation between 0 degrees and -6 degrees vertical angle for different simulations with cold windows over a range of cold bore pressures from 28 to 100 mbar at 1.8K. The comparison of laminar (when horizontal) and half-laminar (when tilted) reproduces the experimental trend observed, while comparison of turbulent (horizontal) and half-laminar (tilted) does not. The hydrostatic and magnet temperature corrections have been subtracted from the points.

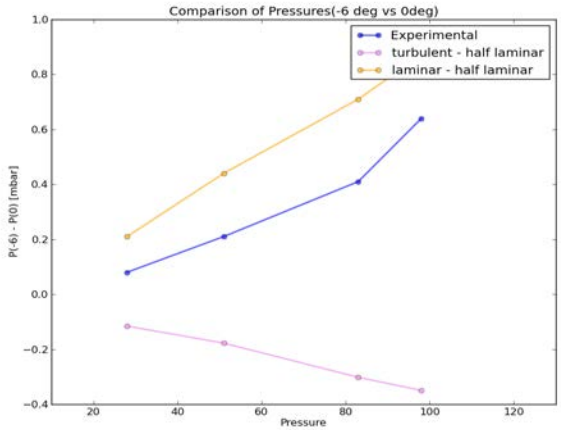

Figure 33 - Experimental and simulated pressure variation for cold windows between -6 degree and 0 degrees, after removing effects of temperature excursion and hydrostatics.

The experimental points favor a laminar (horizontal) – half-laminar (tilted) over the turbulent (horizontal) half-laminar solutions. Indeed half-laminar solutions are the only ones which create a significant pressure variation with angle and comparing the experimental and simulated pressure changes within a half-laminar model in different tilting angles, one gets a better agreement with experimental data (Figure 34).

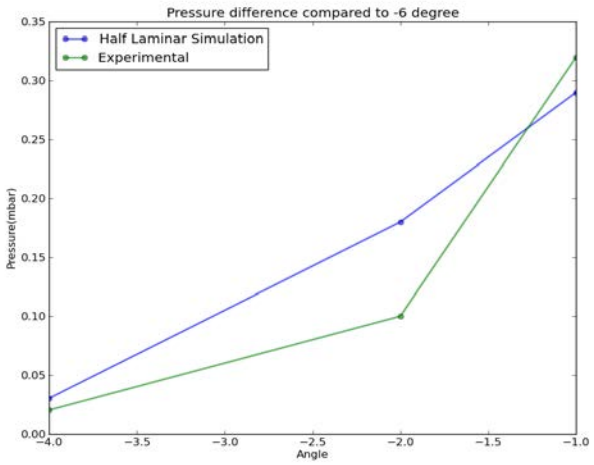

Figure 34 - The pressure change with respect to -6 degrees, after removing effects of temperature excursion and hydrostatics. The change predicted by the half-laminar simulation is in agreement with the experimental data within 0.08 mbar.

The offset between experimental and laminar (horizontal) – half laminar (tilted) suggests that whilst the horizontal laminar is nearer to reality than the horizontal turbulent model, the horizontal laminar slightly overestimates the number of moles needed to reproduce the measured pressure resulting in an offset of ~0.2 mbar compared to experiment. For instance for the simulations of horizontal magnet at 83 mbar, the laminar model predicts 19.52 moles while turbulent model predicts 19.27 moles.

The success in reproducing the pressure variation trend during tilting justifies our assumption that the gas dynamics play a significant role in the pressure variation observed. Our analysis procedure continuously corrects to the center of the magnet the measured pressure for the hydrostatic and the magnet temperature variation (via the 3He equation of state). Figure 35 shows the various contributions from CFD to the pressure variation on tilting to -6 degrees compared with experimental value.

Whilst the CFD justifies our approach, CFD is not used in calculating the central gas density during each solar tracking. The pressure variation observed causes a spread in the central density value and hence the mass coverage for each setting. The intrinsic resolution of ~1 meV is widened to 4 meV at high densities allowing an increase in step size.

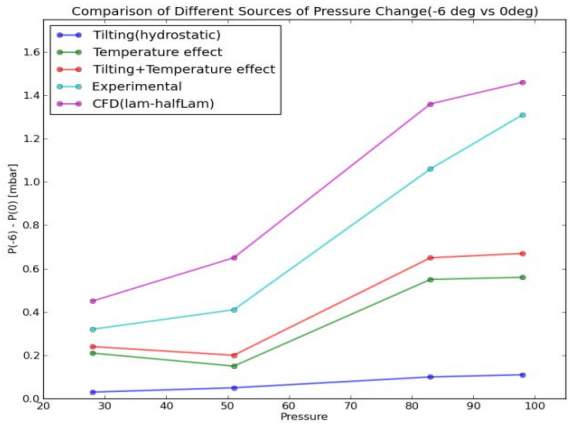

Figure 35 - Source of the pressure change during tilting comparing -6 degree and horizontal cases.

2.4 Data taking, analysis and publications

After a successful end of CAST data taking with helium inside the magnet bores, the data taking program in 2013 is dedicated to repeating, with significantly improved sensitivity, the measurements with vacuum inside the magnet bores. The data taking started on 22nd September and will last until 10th December. The detectors used for the 2013 data taking are three Micromegas detectors (two on the sunset side and one on the sunrise side) and a new SDD detector on the sunrise side. The data taking efficiency, in terms of solar trackings covered, is 85% (for the period 22nd September to 11th October).

The ^{3}He part of the CAST data (data-taking periods 2009-2011) corresponding to the interval $0.64 \leq m_a \leq 1.16$ eV has been analyzed almost fully. The three Micromegas detectors do not report any excess of counts that would correspond to a signal, which leads to the restriction of the axion-to-photon coupling constant to values below 3.3×10^{-10} GeV^{-1} at 95% CL, with the exact value depending on the pressure setting (see Figure 36). The estimation of the possible effects the tilting of the magnet may have on the density along the magnet bores has been conservative, while more work to refine the model is in progress. A publication has already been submitted to Physical Review Letters and is currently in the review process [4]. The analysis of the data taken with the CCD is currently ongoing.

In 2012, data were collected with the magnet bores filled with ^{4}He, in improved conditions with respect to the 2006 run, revisiting a narrow part of the axion mass range around 0.4 eV. The three Micromegas detectors do not report any excess of counts that would correspond to a signal, which leads to the restriction of the axion-to-photon coupling constant to values below 1.5×10^{-10} GeV^{-1} at 95% CL, with the exact value depending on the pressure setting (Figure 37). The analysis of the data taken with the CCD is currently ongoing. Preparation of the publication is about to begin.

As a by-product, CAST derived limits on the product of the axion-to-electron and axion-to-photon coupling constants using the CAST phase I data (vacuum phase) and the results were published [5]. The analysis excludes the region above the thick black line in Figure 38.

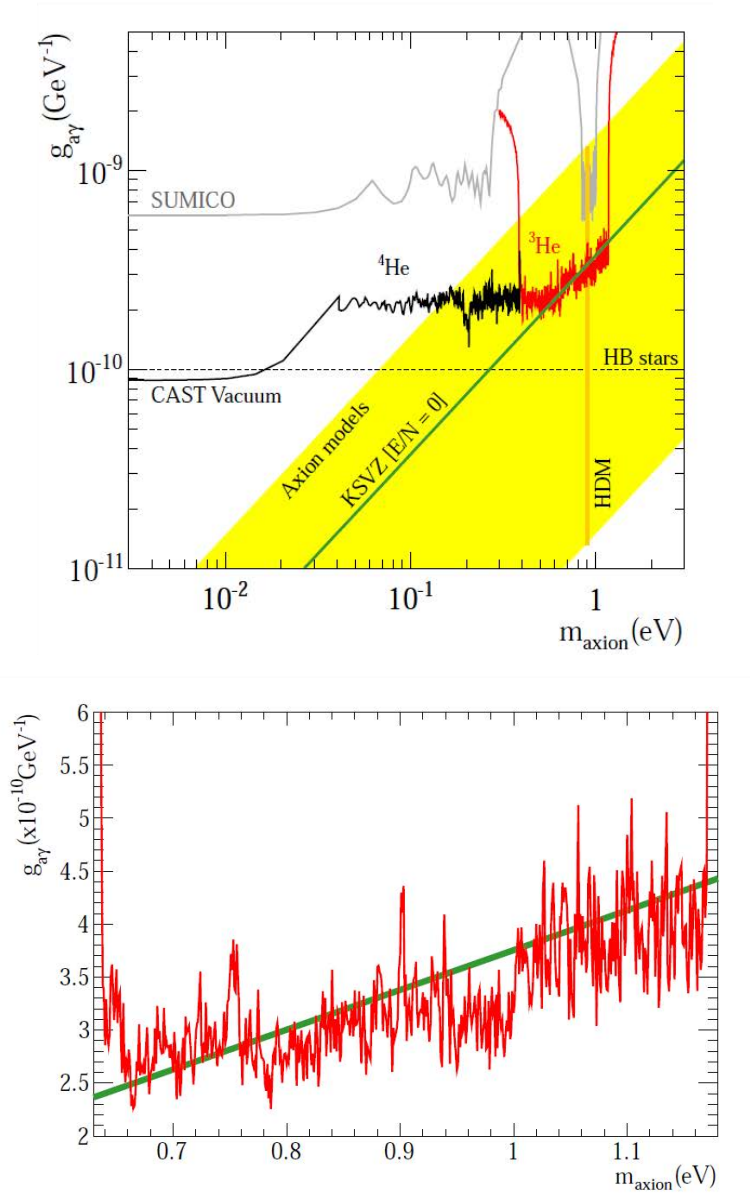

Figure 36 - *Top:* Exclusion regions in the m_a-$g_{a\gamma}$ plane of the CAST results during the vacuum, and 2005 ^{4}He phase (black). In red the results for the ^{3}He phase, (above 0.64 eV computed with the data of 3 out of 4 detectors). *Bottom:* Expanded view of the preliminary limit for ^{3}He phase for axion mass range between 0.64 and 1.18 eV. Only 3 out of 4 detectors have been computed.

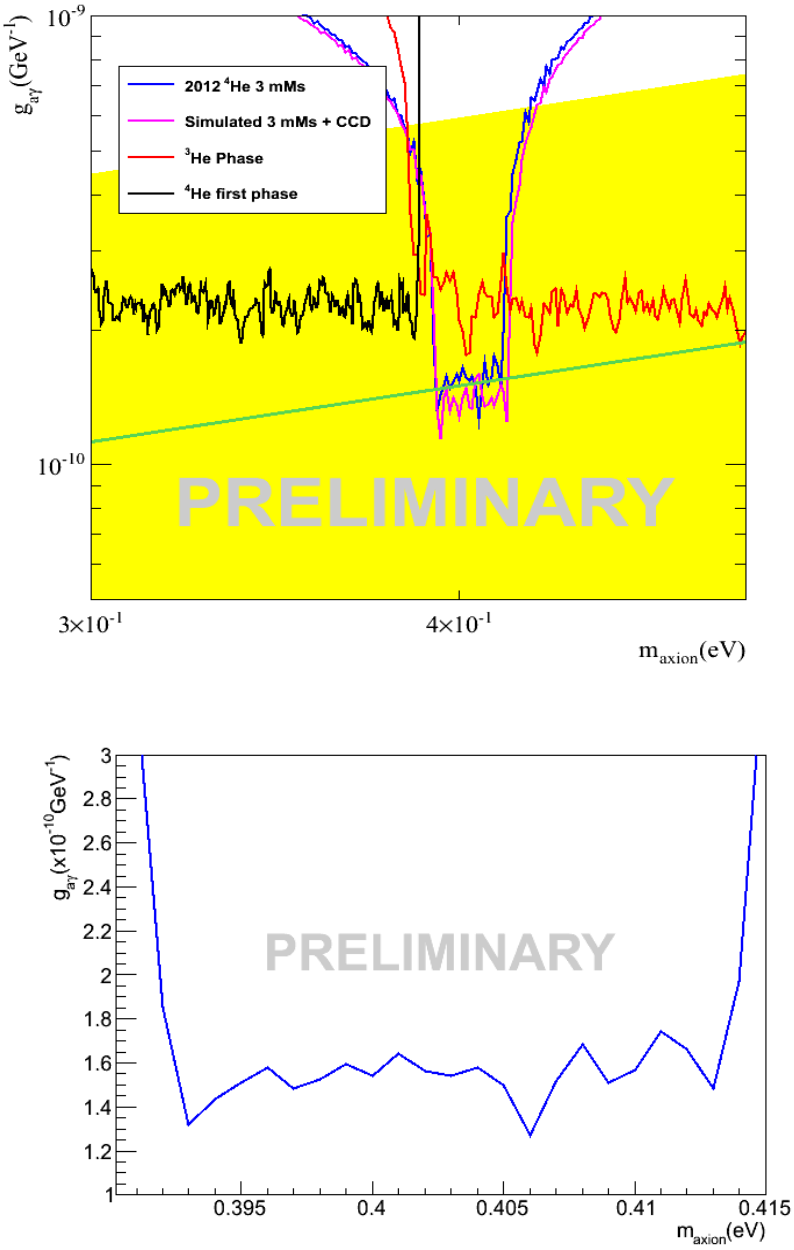

Figure 37 - *Top:* Preliminary results of the ^{4}He data taken during 2012 with 3 out of 4 detectors (blue), compared with the expectations for all CAST (pink). *Bottom:* Expanded view of the top plot.

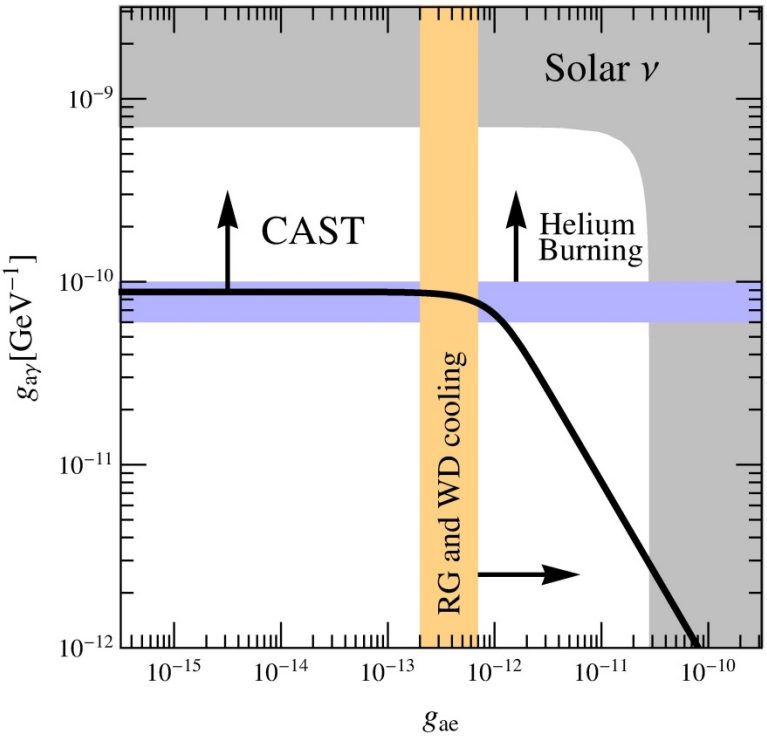

Figure 38 - Constraints on the axion-to-electron (g_{ae}) and axion-to-photon ($g_{a\gamma}$) coupling constants for m_a<10 meV. The region above the thick black line is excluded by CAST. The grey region is excluded by solar neutrino measurements. In the vertical orange band, axion emission strongly affects white dwarf cooling and the evolution of low-mass red giants; parameters to the right of this band are excluded. Likewise, helium-burning stars would be perceptibly affected in the horizontal blue band; parameters above it are excluded.

2.5 Paraphotons

The BaRBE low energy photon detector system has been taking data on the CAST VT3 beamline until October 2012, as detailed in previous reports to the CERN SPSC. The sun-tracking and background data collected by BaRBE in 2010, 2011 and in 2012 have been analysed to determine a Dark Count Rate (DCR) which was then used to obtain an experimental bound on the production of paraphotons in a vacuum section of the beampipe in front of the BaRBE detector. Figure 39 below shows a schematic drawing of the apparatus geometry relevant for the detection of paraphotons. The unrestricted vacuum fiducial volume in front of the BaRBE semitransparent mirror, which conveys photons to the collection optics and then to the detector by means of an optical fiber, has a length of 70 cm.

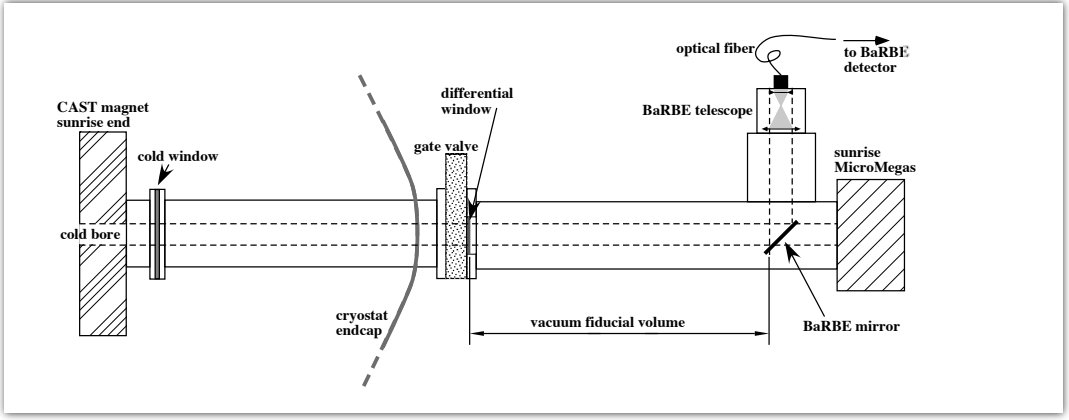

Figure 39 - Schematic drawing of the apparatus used to collect the BaRBE data (see text).

The detector used for these measurements is a photomultiplier tube (PMT) with peak sensitivity at 3.5 eV, also described in previous reports. Thanks to the presence of an optical switch at the end of the optical fiber before the detector, the PMT looks for half the time at the fiducial volume ("Light" state) and for another half at a shutter ("Dark" state). Since switching occurs at a frequency of 1 Hz, it is safe to assume that the "light" and "dark" states share a common background, which can then be subtracted to achieve a final DCR.

Data were acquired each day during CAST sun-tracking runs for 5500 s, followed by 72000 s of background data with the magnet in parking position. In 2010-2011 the BaRBE setup acquired data for a total of $8.7 \cdot 10^5$ s during sun-tracking and for $1.17 \cdot 10^7$ s when measuring background, all with an angular Field Of View (FOV) of 1 mrad. In 2012 the FOV was increased to 7.5 mrad and the data taking times were $1.5 \cdot 10^5$ s sun-tracking, $1.9 \cdot 10^6$ s background.

The final DCRs obtained by BaRBE for sun-tracking data are 1.4 mHz in 2010-2011 and 3.5 mHz in 2012. These results have been used by to obtain the preliminary exclusion plot for the kinetic mixing of paraphotons with ordinary photons reported in Figure 40 (theoretical calculations by S. Troitsky, INR Moscow). A publication on this topic is in preparation at the moment.

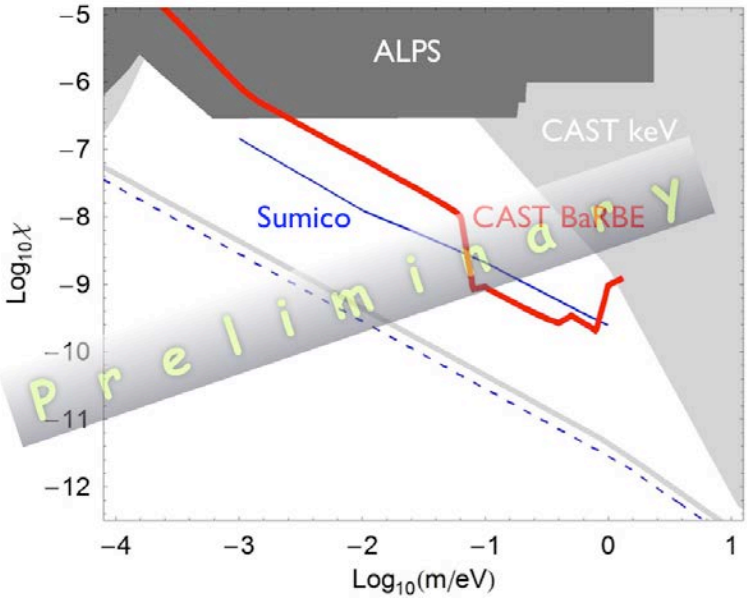

Figure 40 - Exclusion region in the mass-kinetic mixing plane for paraphotons obtained from the BaRBE 2010-2012 data. The red solid line represents the CAST BaRBE bound, while the blue line gives the bound published by the Sumico collaboration[6]. The blue dashed line and the grey solid line represent bound calculated in [7] from other experimental data using a different theoretical model (longitudinal mode).

2.6 Sun filming and GRID measurements

2.6.1 Sun filming

Twice a year it is possible to check the precision with which the magnet is pointing at the Sun with a direct, visual method. It consists of taking pictures of the Sun in a special sun filming solar tracking run, with a camera with a high precision lens attached to the magnet. This camera is precisely aligned with surveyors help to the V1 bore of the magnet. Also, an atmospheric refraction correction is applied into the vertical motion, because of the difference between axions and photons propagating through the atmosphere.

Unfortunately, the Sun filming can only be made in a 10-day period twice each year. Success is totally dependent on the weather conditions. When misty or cloudy, it can make the analysis of the pictures difficult and less precise, and if overcast - impossible to visualise the sun. In the September 2013 campaign, the weather has been favourable and a total of six days have been useful for analysis (Figure 41).

For the alignment of the camera to the bore of the magnet, a setup of two irises (one in front of the camera, and the other one in a corner of the hall) and a laser are used to create an optical axis, which is then aligned to the aforementioned V1 bore with the help of the CERN surveyors.

This year the camera support bench has been modified to offer more stability. For this purpose, an old unused filming system has been removed and the current system has been installed on its place. This has implied moving the camera transversely towards the magnet

by about 20 cm compared to its previous position. The laser platform on the other side of the hall has been adjusted to take into account the camera movement.

During filming, the camera is controlled remotely from a PC, where it is possible to adjust the necessary parameters of exposure and sensitivity to obtain good quality pictures. These are taken as frequently as possible, around ten pictures per minute. After that, the analysis is done using the *NI Vision* LabView module for image analysis. In this analysis, the centre of the Sun is extracted from every picture, along with the radius of the Sun and the goodness of the fitting analysis.

Figure 41 - Example of a picture of the sun from the 21st of September.

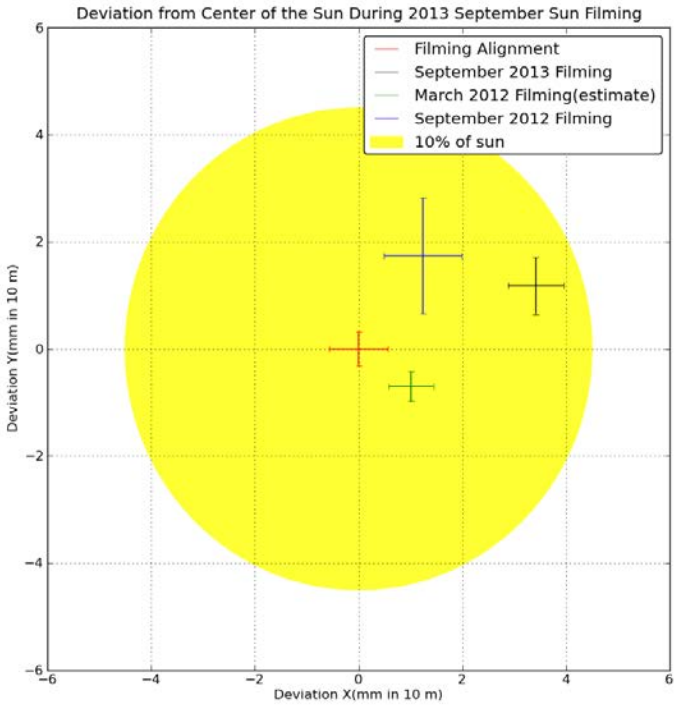

Figure 42 - Results of September 2013 and previous filming campaigns.

The results of this campaign show that we are pointing at the Sun: (3.4 mm)/(10 m) ahead of the centre and (1.2 mm)/(10 m) above it. Figure 42 illustrates this result together with two previous filmings: March 2012 and September 2012. Whilst still within 10% of the centre of the Sun, we observe a small shift away from the centre compared to the 2012 filming. Unfortunately, on March 2013 the sun filming could not be done due to ongoing work on the magnet.

Although the magnet has a different weight distribution, due to the new detector shielding, this cannot explain this difference. Also, a new full Grid has been done in September 2013 to consider this new weight distribution (the Grid procedure is explained in more detail in the Grid section).

The most plausible explanation for this deviation is an error in the alignment of the camera with respect to the V1 bore of the magnet. Indeed the alignment of the irises was checked after several days of filming and a movement of several mm in the iris in the corner of the zone was found necessary. The reference checks done each day during the filming were stable and reproducible.

The first half of the present filming campaign was done with the 2011 grid input into the tracking program, the same used in the 2012 run. In the middle of the campaign, however, we changed to the recent 2013 grid. This new grid gives a correction of (0.5 mm)/(10 m) horizontally in the movement of the magnet and brings us closer to the Sun, as shown in Figure 43.

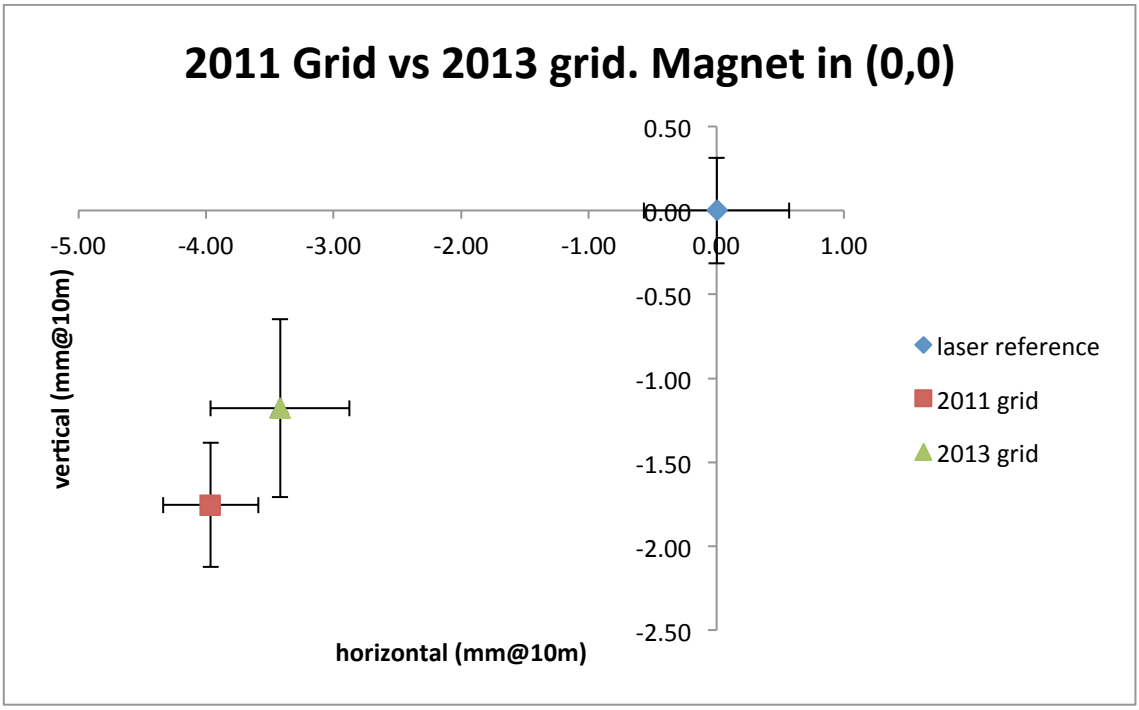

Figure 43 - Comparison between 2011 and 2013 during this filming campaign.

The present result for solar alignment shows the magnet leading the sun by 3.4 mm in 10 m horizontally, and above the sun by 1.2 mm in 10 m vertically. This results in a radial offset of

1.24 arc-minutes, while for operation with the XRT the alignment should be better than 1.0 arc-minutes. However, since the 2013 run will not include focusing optics, the present alignment is to be considered adequate. Studies will continue to understand the discrepancy.

As an additional tool to study the magnet alignment, lunar filming is being studied as it presents many more opportunities for filming during the year. It is not yet known if the tracking program can be trained to follow the moon.

2.6.2 GRID 2013

CAST performs periodically the so-called GRID measurements with the help of the team of geometers from CERN. This consists of the independent measurement of the position of the magnet in a set of reference coordinates (GRID) previously defined to cover all reasonable movements of the magnet. These measurements are intended to detect any drift in the pointing ability of the system with respect to the reference calibration currently used by the tracking software and change the reference calibration if necessary.

During the data taking of 2012, the 2011 grid was used as the reference calibration. The data taking of 2013 started the 22nd of September with the 2011 grid, but on the 25th of September, the new 2013 GRID replaced the 2011 in the tracking program.

The 2013 GRID was performed at the same 90 points that were originally used in 2011 grid, and difference of each measurement in vertical and horizontal angles are calculated. The difference in vertical angle measurements are within ±0.5 mm, while horizontal angles in 2013 grid differ by maximum +1.58 mm in 10 m, and minimum -0.72 mm in 10 m as in Figure 44 and Figure 45.

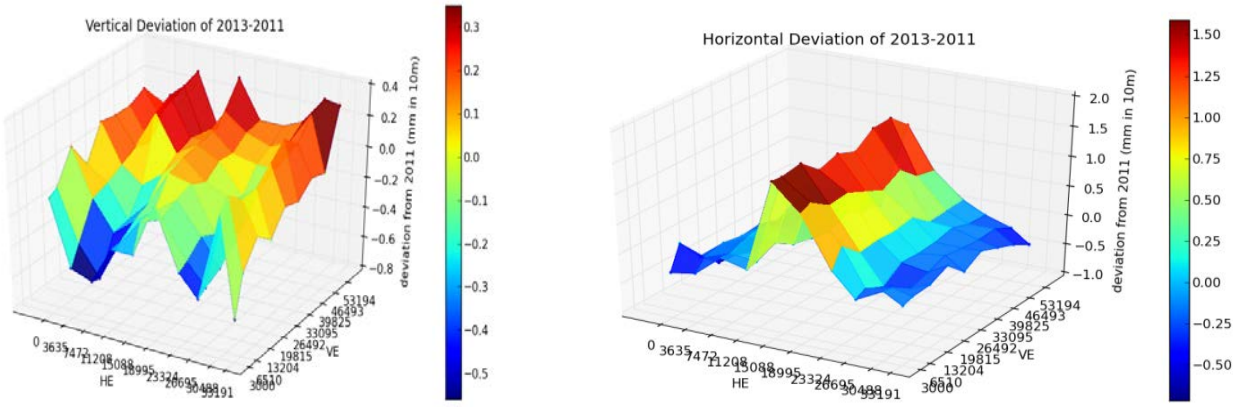

Figure 44 - Vertical and Horizontal deviations of 2013 and 2011 GRID measurements

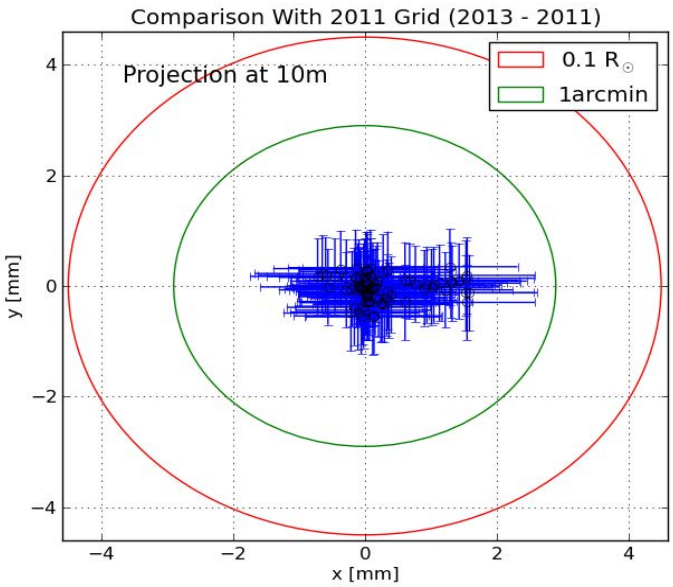

Figure 45 - Vertical and Horizontal deviations of 2013 and 2011 grid measurement together with the circles showing 1 arc-minute and 10% of the Sun.

3 Proposal for 2013 - 2014

3.1 Upgrades, Planning & Requests

3.1.1 Micromegas detectors upgrades for 2014

As it is explained in Section 3.2, the vacuum run in CAST in 2014 will allow testing a dedicated x-ray focusing device coupled to a Micromegas detector. This will mean the merging of the two main CAST innovations regarding low energy x-ray detection, and will yield an increase of sensitivity. The x-ray photons produced by back-conversion of solar axions in the CAST magnet will be focused in a spot of a few mm^2, in comparison with the current sensitive area of 14.5 cm^2 (see comparison in Figure 46). This represents an increase in signal-to-noise ratio of around a factor of 10^2. It is worth noting that the x-ray window diameter will be much smaller, and so will be the outer diameter of the vacuum pipe that couples the detector to the x-ray focusing device. This fact, together with the shift of the focal point with respect to the magnet axis introduced by the optics, removes many of the mechanical constraints that did not allow designing an efficient enough shielding. The lead shielding for the sunrise side for 2014 is designed to be around 10 cm thick, instead of the ~5 cm of the present setup, and it will be extended by a few tens of centimeters along the vacuum pipe providing better solid angle coverage. In addition, the vacuum pipe will be made out of copper (with a PTFE coat in the inner surface to block the 8 keV fluorescences) instead of stainless steel (whose fluorescence lines are in the 5-7 keV range, inside the CAST RoI). Finally, the results from the Sunset MM setup and the test-benches motivate the installation of a new custom-made scintillator veto to identify cosmic events.

At the Sunset detectors, the drift cathodes installed for 2013 were made out of aluminum instead of copper due to technical difficulties with the last ones. As it is reported in Section 2.2.3 the contribution to background of the aluminum cathode was ~5×10^{-7} $keV^{-1}\cdot cm^{-2}\cdot s^{-1}$ due to its internal radioactivity, so with this replacement the background level in the CAST RoI will very likely reach ~10^{-7} $keV^{-1}\cdot cm^{-2}\cdot s^{-1}$, i.e. a background level as low as those obtained underground.

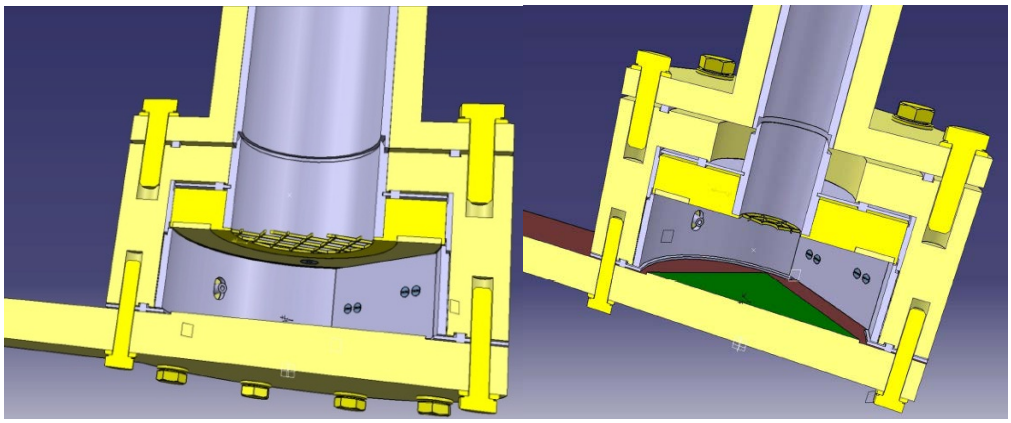

Figure 46 - Comparison of current (left) and future (right) sunrise Micromegas chamber design.

3.1.2 New Optics

A consortium consisting of Columbia University, the Danish Technical University-Space (DTU-Space) and Lawrence Livermore National Laboratory (LLNL) will oversee the construction of the new X-ray telescope for CAST. The team will leverage the significant infrastructure, expertise and close teamwork developed during the design, fabrication and calibration of X-ray optics for the Nuclear Spectroscopic Telescope Array (NuSTAR[1],[8]), a NASA small-explorer satellite successfully launched in June 2012. NuSTAR is the first observatory in space using focusing optics to image the sky in the energy range of 5-80 keV).

Figure 47 - NuSTAR X-ray telescope during on-ground calibrations at Columbia University. The optic, which is a conical approximation to a Wolter-I telescope, consists of 6 sectors. The supporting spider structure can be seen in the right part of the image. For CAST, only one sector of a NuSTAR-like optic needs to be built.

In order to achieve high throughput (X-ray astrophysicists refer to this as high effective area for a telescope) in this pass-band, NuSTAR telescopes (see Figure 47) required several innovations over previous generations of X-ray telescopes. First, a new-type of lightweight, high-quality, low-cost substrate was required. Second, the physical configuration of the telescope and the mirror coatings had to be developed and third, the coated mirrors needed to be integrated in a single telescope assembly.

- The final solution for the substrates was to take float glass originally developed for flat-panel screens (e.g., the display in laptops or hand-held devices), and thermally heat or "slump" the glass into the appropriate shape (approximately 1/6th or 1/12th of a truncated cone). Columbia University, the PI institution for the NuSTAR x-ray telescopes, pioneered this approach for manufacturing substrates.
- Next, scientists from all three institutions developed the optical prescription (i.e. the physical configuration and dimensions of the telescopes) and designed the specialized

[1] www.nustar.caltech.edu/
http://www.nasa.gov/mission_pages/nustar/main/index.html

coatings that are applied to the glass substrates to enhance reflectivity at hard X-ray energies. Multilayers, alternating layers of high- and low-density (and high- and low-atomic number) materials, act like synthetic Bragg crystals. For NuSTAR, multilayer coatings are deposited via magnetron sputtering. DTU-Space developed custom facilities to clean the substrates and deposit extremely uniform, well-controlled and stable coatings.

Finally, these coated mirror substrates had to be integrated into a single telescope assembly. In the case of NuSTAR, the final telescope consisted of 133 nested layers with more than 2000 individual mirror segments. The assembly philosophy and the custom integration machines were conceived, designed and utilized by Columbia University staff, with additional support provided by LLNL.

Columbia, DTU-Space, LLNL and other institutions first built optics using the approach described above for a balloon mission called HEFT, before NuSTAR was funded by NASA. The teams have been working together for more than a decade, and the optic for CAST will utilize all of the existing facilities and tooling.

The baseline plan for the CAST experiment is to build a single optic that will be coupled to a Micromegas detector of the latest generation. The telescope will be integrated on the existing Sunrise Micromegas line. To first order, this new optic will have properties similar to that of the ABRIXAS X-ray telescope already employed by CAST. It is important to note that due to the fact that the approach for building a new CAST optic differs fundamentally from manufacturing NuSTAR telescopes, the new optic for CAST will be much easier to build than a NuSTAR optic. Specifically, the telescope will consist of only 15 nested shells. Additionally, since the CAST magnet bore is small (diameter of 43 mm), there is no need to construct a complete telescope. It will be sufficient to build 1/6th of a full NuSTAR optic, i.e. one of the six mirror sectors. This implies that the total number of substrates required for two reflections will be only twice the number of layers or a total of 30 individual mirror segments. Figure 48 illustrates the design of the new optics in front view as seen from the SR MM direction. The maximum width and height of the complete CAST X-ray optic (support mandrel and one telescope sector) have been determined to be 200 mm and 150 mm, respectively. This is mainly due to space constraints in the experimental setup of CAST. The illustration shows the mirror segments and the building mandrel in dark grey. A yellow circle indicates the size of the CAST magnet bore.

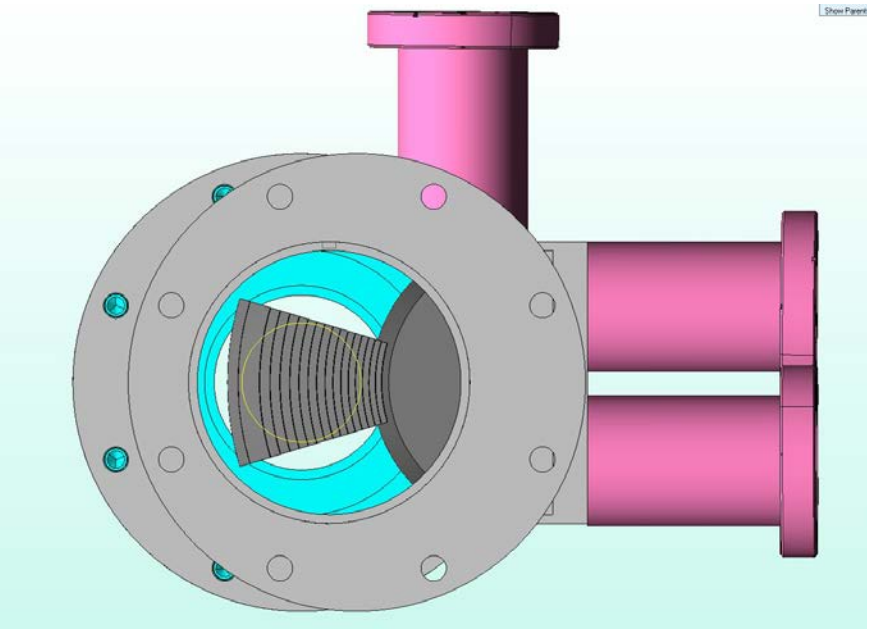

Figure 48 - Schematic view of the new X-ray optic for CAST. The 1/6 mirror pack of a full NuSTAR optic is shown in dark grey and the size of the CAST magnet bore is indicated by the yellow circle. The building mandrel of the optics can be seen in dark grey to the right of the mirror stack.

Figure 49 shows a close-up schematic view of the X-ray telescope: The angle of each glass substrate depends on the focal length, l, and radius, r, and is described as $\tan 4\alpha = r/l$. Every layer put on the mandrel has to have a width wide enough to cover the bore opening which sets a lower limit on the radius of the innermost glass layer. Each subsequent glass substrate is mounted on top of the earlier so there is no overlap. The resulting diagram for an optic optimized for a 43 mm bore opening and 1.5 m focal length is shown. The right side of Figure 49 shows a side view of the optics. Two sets of mirrors with 15 shells each focus the putative axion signal from the magnet bore (left) onto a small spot on the Micromegas detector (right). The spot size cannot be calculated a priori, since it requires detailed metrology data of the mirrors. Using NuSTAR performance information, it can be estimated, however, that an extraction region of 4-arcmin radius would contain 80% of the encircled energy.

An optimized coating recipe for the multilayers is being developed, considering material combinations of W, Pt, Ir or Ni with Si, B_4C or C. A given material combination along with a given number of coated layers and thicknesses of each layer yields a specific reflectivity. The integrated value of the coating along with the detector quantum efficiency and axion spectrum is used to find the optimal coating recipe of each glass substrate layer in the optic (see Figure 50). The coatings will be deposited using a designated magnetron sputter facility at DTU Space, also used to produce all coatings for the NuSTAR mission. Each glass layer can be coated with a separate coating recipe. To safe time it is also possible to use only a few coating recipes for the optic, but resulting in a slightly decreased reflectivity.

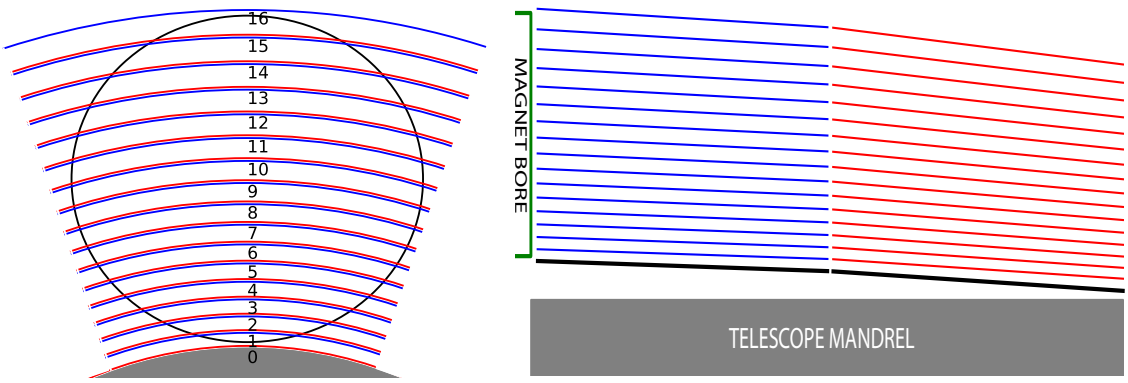

Figure 49 - Diagrams of glass layering in Wolter I optic for the CAST axion helioscope. Left: Optic as seen from front. The circle shows the magnet bore opening compared to the optic. Right: Optic seen from side. Horizontal axis is compressed to show the tilt of each glass layer.

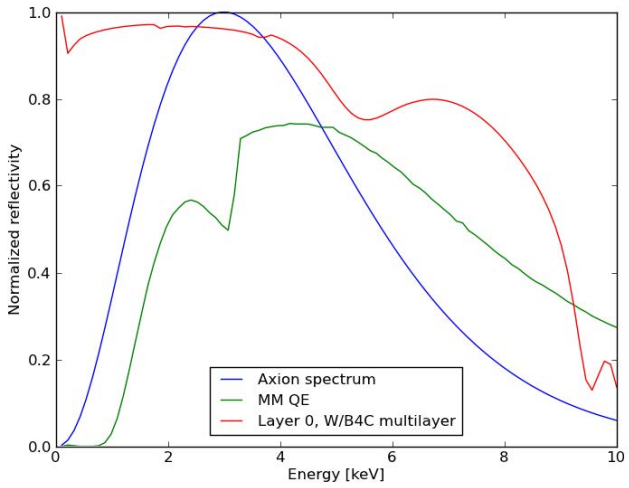

Figure 50 - Reflectivity (red) of a given coating recipe of a glass layer, compared to the normalized axion spectrum (blue) and detector quantum efficiency (green).

Currently the optics prescription is being finalized with the optimization process of coating recipes close to completion. The baseline approach is to use W/B_4C for the multilayers. The next step is to fabricate the support structure, coat the glass with the derived recipe at DTU and build the optics on top of a mandrel at LLNL using the NuSTAR assembly machines (Columbia U.). Once the optic is complete, we will validate the base performance using an x-ray tube, before installing the telescope at CAST. A full calibration is scheduled at PANTER following data acquisition at CERN.

Assuming availability of all required facilities for building and calibrating the new X-ray telescope, we anticipate to order material, set up the support structure and complete the coating process by the end of Q4 2013. The optic could then be assembled and tested in Q1 2014. This would position us to have a telescope ready for science observations at CAST in Q2 of 2014.

3.1.3 Radiation pressure from solar chameleons

The principle of kinetic detection of chameleon-type WISPs is based on their density dependent interaction with matter (see [9] for a more detailed discussion on chameleons). In particular, a flux of solar chameleons will exert the equivalent of a radiation pressure on a solid surface of appropriate density. If placed at a grazing incidence angle with respect to the chameleon flux, the micro-membrane will be subject to a radiation pressure displacing it from its equilibrium position and exciting its vibrational states. Sub-nm movements of such membranes can be detected by placing them inside a Fabry-Perot (FP) optical resonator [10]. High sensitivity to membrane displacements can be reached by exploiting the multiplication factor afforded by the finesse (resonator Q in practice) of the FP. During operation the FP is kept at resonance with a probe laser beam by means of a feedback loop: the control signal of this loop contains the information on membrane motion, and hence, on (solar) chameleon properties.

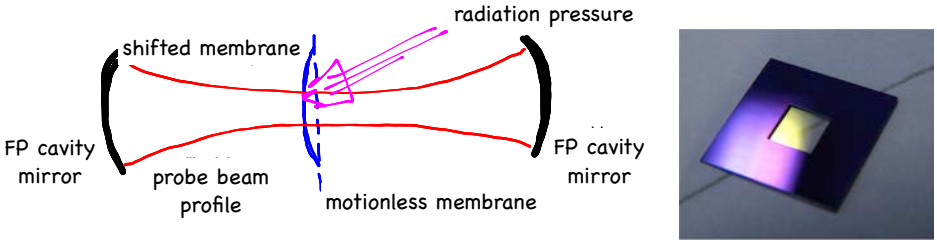

Figure 51 - Sketch of the membrane in a cavity principle. Membrane displacements (solid blue line) with respect to the motionless state (dashed blue line), in response to an external pressure, will modify the spatial modes of the probe beam. Their frequency changes are corrected by the cavity control loop, and can be detected from the loop error signal (left). Example of a (1 mm)x(1 mm), 50 nm thick Si_3N_4 micro-membrane mounted on a 200 μm thick Si substrate (right).

A prototype radiation pressure opto-mechanical sensor (called KWISP) with a micro-membrane placed inside a FP cavity has already been built at INFN Trieste, using existing equipment and mechanical pieces custom made in house, and is currently undergoing optimization of the optical setup to ready it for sensitivity tests[18]. Figure 52 shows a photograph of the prototype inside it vacuum chamber while aligning the various optical elements.

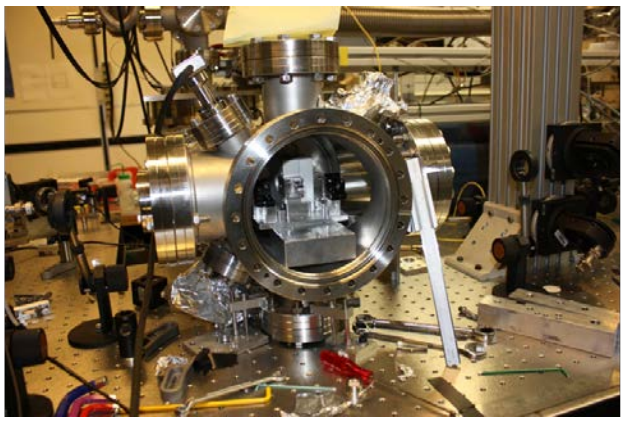

Figure 52 - Photograph of the KWISP opto-mechanical force sensor prototype during alignment of the optics at INFN Trieste (see also text).

The sensitivity of the KWISP prototype to an external radiation pressure will be tested by subjecting the membrane to the pressure exerted by a laser beam, while monitoring the membrane movements with a second probe beam. The optical setup is schematically shown in Figure 53.

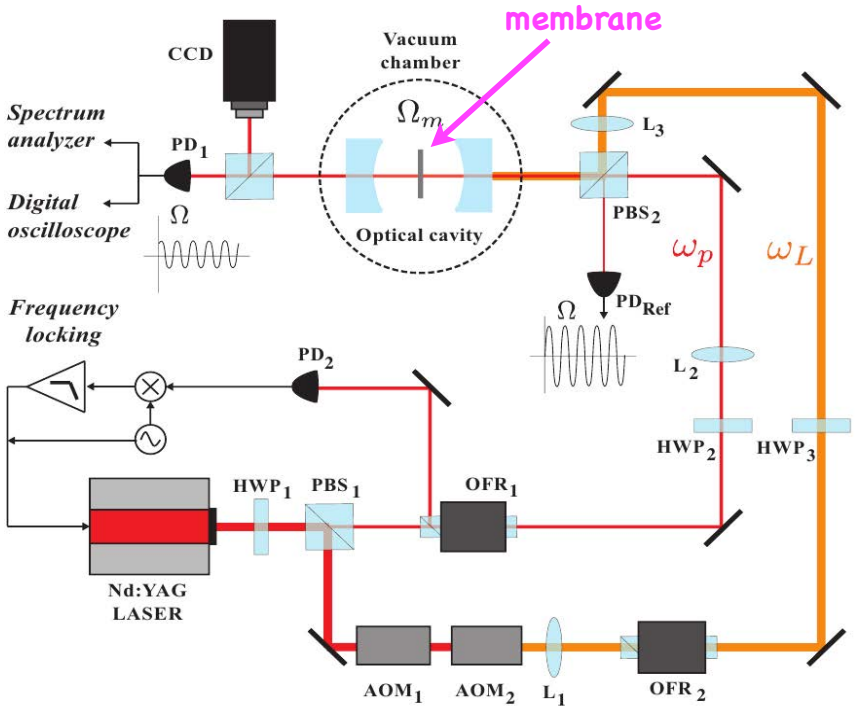

Figure 53 - Scheme of the optical setup for measuring the sensitivity of the KWISP detector to an external force impact The probe beam (ω_p) at 1064 nm, which is frequency-locked to the FP cavity and transmitted through it, senses membrane movements. For calibration purposes, the intense, frequency-shifted, pumping beam (ω_L) exerts a controlled radiation pressure on the membrane.

Once tested at INFN Trieste, the KWISP prototype can be transferred to CAST and attached to the focal plane of the X-ray telescope, optionally replacing the X-ray detector. This will be the first solar chameleon measurement with a flux enhancement by a factor ~100-1000 compared to the laboratory test measurements.

While preparing the FP-based sensor, a preliminary series of measurements was carried out on a simpler configuration to obtain an initial estimate of the displacement and force sensitivity of such a device. The available membrane [11] was placed, under vacuum, in one of the arms of a Michelson-type interferometer to act as a mirror, since it is reflective at the 532 nm light wavelength used for these tests. The other interferometer arms contained a moveable mirror mounted on a PZT actuator. Figure 54 shows an image of this Michelson-type interferometer setup. In this scheme, changes in the lengths of the two arms, due for instance to mirror movements, result in a shift of the interference fringes which form at the interferometer output. In particular, a shift from a bright fringe to the next dark one, corresponds to a change in length of half wavelength (= 532/2 nm).

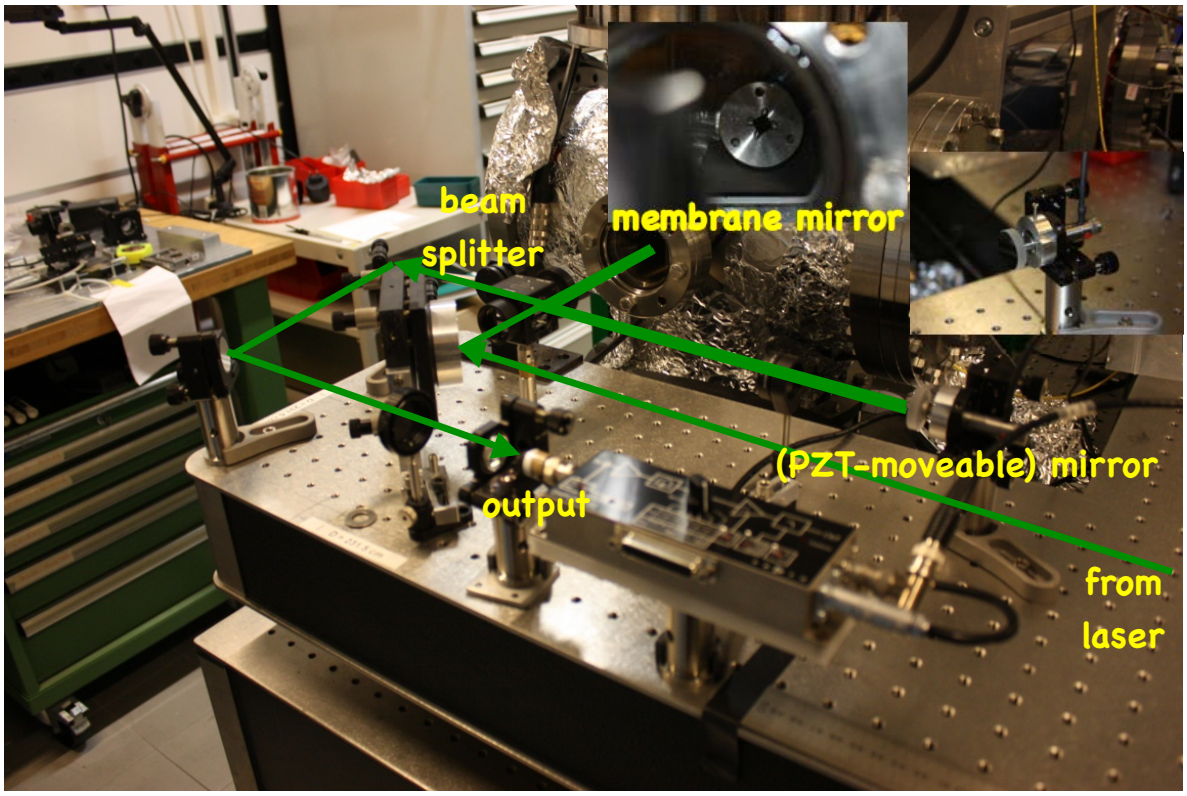

Figure 54 - Setup of the bench-top Michelson-type interferometer for preliminary testing purposes. The membrane, acting as a mirror at 532 nm, is placed inside a vacuum chamber and is illuminated through a window (upper center), forming one arm of the interferometer. The other arm is formed by a moveable mirror mounted on a PZT actuator (center right).

Two types of measurements were carried out :

i) the membrane was excited with a transient mechanical vibration by simply hitting the optical bench and the corresponding intensity variation at the interferometer output was recorded on the oscilloscope;

ii) with the membrane stationary, the PZT moveable mirror was excited with a sine wave at a given frequency and the corresponding amplitude in the output intensity Fourier spectrum was recorded.

In case i) the maximum excursion recorded at the output was 276 μV, and therefore the characteristic of the system is $C = (276\ \mu V)/(532\ nm/2) = 1.0\ \mu V/nm$ (see Figure 55).

In case ii) the membrane was kept stationary and simply used as a mirror and the PZT-mounted mirror was moved in controlled way by means of a sine wave signal. To determine the PZT transduction characteristic a 100 Hz sine wave was fed to the PZT. With a 600 mV_{p-p} amplitude the output shifts from one bright fringe to the next, corresponding to a full wavelength. Therefore the transduction characteristic of the PZT is $D = (600\ mV)/(532\ nm) = 1.1\ mV/nm$. This is an intrinsic parameter of the piezoelectric actuator and should not be confused with the response characteristic C measured above.

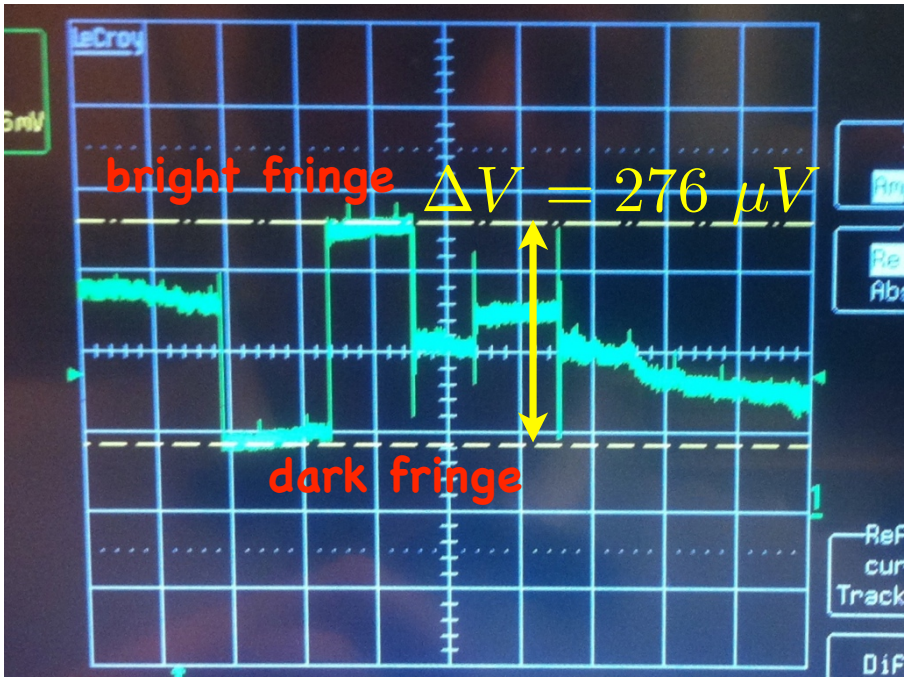

Figure 55 - Oscilloscope trace recording of the interferometer output intensity excursion in response to a fringe shift (see text).

Subsequently, to estimate the displacement sensitivity at frequencies as near as possible the mechanical resonance frequency of the membrane (~400 kHz), the PZT was excited with a 10 kHz, 13 mV sine wave (the frequency limitation comes from the PZT actuator input bandwidth). The corresponding peak in the Fourier spectrum of the interferometer output intensity was then observed. Figure 56 shows a capture of the spectrum analyzer screen used for this measurement. The peak amplitude at 10 kHz corresponds to the mirror motion amplitude, while the noise floor corresponds to the minimum detectable displacement. The resolution bandwidth of this spectrum is 10 Hz.

A 10 kHz signal having 13 mV amplitude on the PZT actuator then causes a mirror displacement amplitude of (13 mV)·D=14.6 nm. Since the output peak amplitude is 150 μV, the characteristic of the system is (150 µV)/(14.6 nm) =10.3 µV/nm (this characteristic differs from the one given above since it is measured with a more sensitive method). Therefore the observed background level of 6 μV corresponds to a minimum detected displacement of (6 µV)/(10.3 µV/nm)=0.58 nm. This is the first experimental result we achieved in the laboratory before fully implementing the FP-based force sensor.

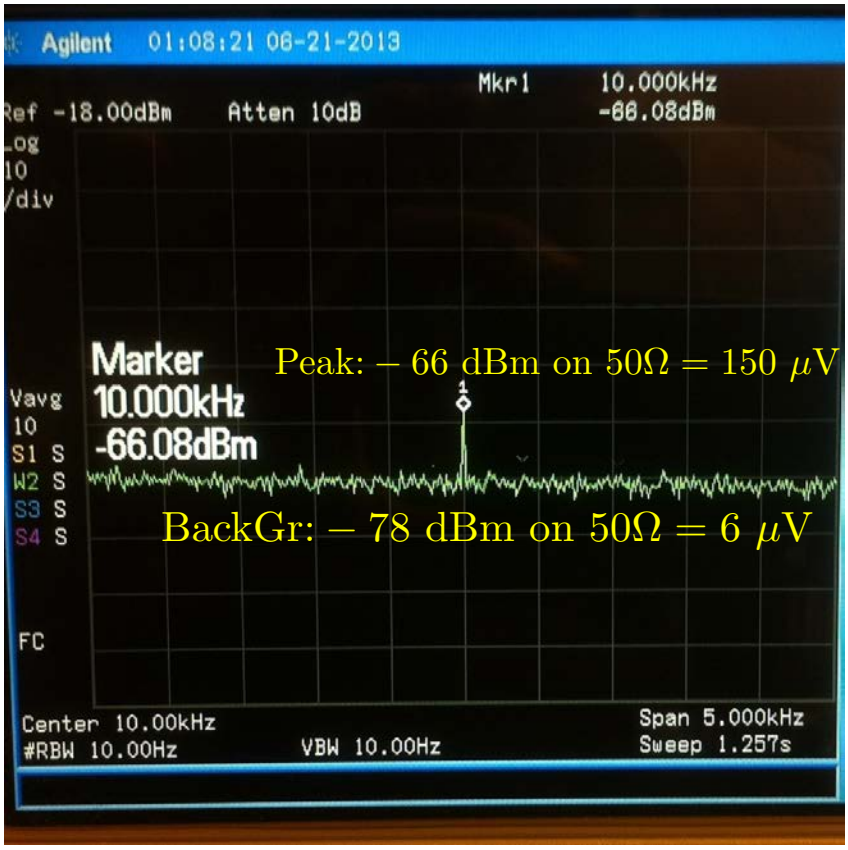

Figure 56 - Screen shot of the spectrum analyzer monitoring the interferometer output intensity Fourier spectrum in response to a mirror motion at a frequency of 10 kHz. The peak corresponds to the mirror motion amplitude, while the noise floor corresponds to the minimum detectable displacement. The resolution bandwidth of this spectrum is 10 Hz.

Given the above result one can obtain the instantaneous displacement sensitivity and, more importantly, estimate the force sensitivity of the Michelson-type system. Since the resolution bandwidth of the Fourier spectrum used to estimate the background was 10 Hz, the instantaneous displacement sensitivity of the test Michelson interferometer is

$$S_{disp} = (0.58\ \text{nm})\left(\sqrt{0.1\ \text{s}}\right) = 0.18\ \frac{\text{nm}}{\sqrt{\text{Hz}}}$$

To estimate the force sensitivity, we used the fact that the micro-membrane used in the previous measurements can be approximated by a simple spring having a spring constant of about 16.6 N/m. This value was obtained by us from a finite-element simulation of the membrane using as input its mechanical characteristics (see Figure 57).

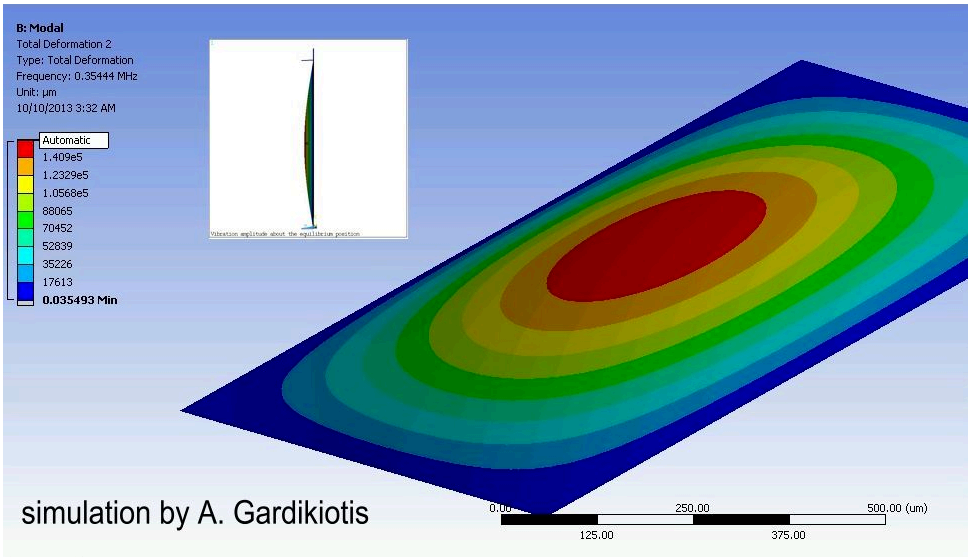

Figure 57 - Finite elements simulation of the fundamental resonance mode of a 50 nm thick, (1 mm)x(1 mm) silicon nitride window (micro-membrane). The obtained frequency (354 kHz) corresponds to the frequency that was experimentally measured. The effective spring constant calculated for this mode is 16.7 N/m.

The resulting force sensitivity is then

$$S_{force} = (16.6\ \mathrm{N/m}) \cdot S_{disp} = 3.0 \cdot 10^{-9}\ \mathrm{N/\sqrt{Hz}}$$

We remark here that this sensitivity is measured using a standard Michelson-type interferometer setup, which, broadly speaking would correspond to a FP resonator with a Q = 1. In other terms, one can expect from the FP-based prototype now under test, which has a nominal Q = 60000, to obtain a projected force sensitivity of

$$S_{force,\,proj} = 5.0 \cdot 10^{-14}\ \mathrm{N/\sqrt{Hz}}$$

This number already compares well with the $10^{-13}\ \mathrm{N/\sqrt{Hz}}$ we predicted last year [9].

Further possible improvement: by cooling the membrane down to the 1 K range one can obtain a further reduction factor of about 100, while a factor 100-1000 in chameleon flux can be gained when working in the focal plane of the CAST X-ray telescope. An overall improvement factor on the above number of 10^4-10^5 is therefore well within reach, without counting further refinements such common mode rejection by chopping the chameleon flux. All these possible improvements will be investigated step-by-step.

3.1.4 TES-based detectors for searches in the eV range and above

Activities in local laboratories regarding the design and testing of Transition Edge Sensor (TES) –based photon detectors have already been introduced in the previous report to the SPSC [9]. These activities have continued in 2013 in the Trieste and University of Camerino, Italy, laboratories [12]. A new TES chip, made by INRIM [13] has been fixed and bonded on a copper base having also a support for mounting the tip of an optical fiber (see Figure 58).

The goal was to control injection of visible photons (1-2 eV) in order to measure efficiency and background.

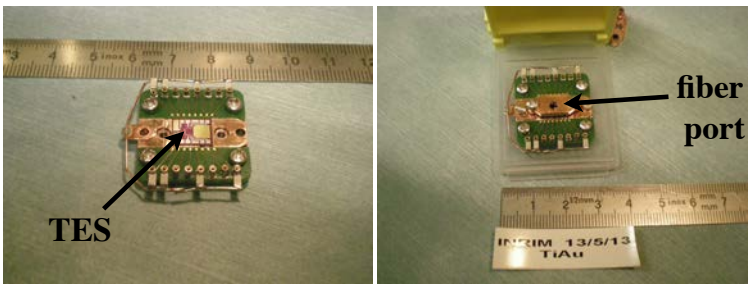

Figure 58 - Ti-Au double layer INRIM TES, 20x20 μm^2 pads, transition temperature 290 mK, mounted and bonded on copper base (at left). Assembly completed with fiber holder port (at right)

The first tests on this sensor, carried out in the spring of 2013, were unsuccessful. We were able to observe the device transition curve and to reduce the RF noise band, which affected 2012 measurements. However, internal oscillations of the electro-thermal feedback necessary for controlling the device resulted in an excessive amplitude noise in response to photon hits. We interpret this as probably due to a non-optimal impedance matching. A second series of tests is foreseen for the end of 2013 – beginning of 2014.

Future developments for the application of TES detectors to (solar) WISP searches are based on the observation that no single device is capable of covering at the same time all the main photon energy intervals to be explored. The characteristics of TES sensors offer a possible solution: integrate on the same chip several sensor pads optimized for different photon energies, and organize the pads in an array to be read in parallel to maximize active area (pads could be arranged side by side (tiled) or sandwiched). To test this concept we propose the Multi Energy TES Array (META) prototype with tiled pads sketched in Figure 59.

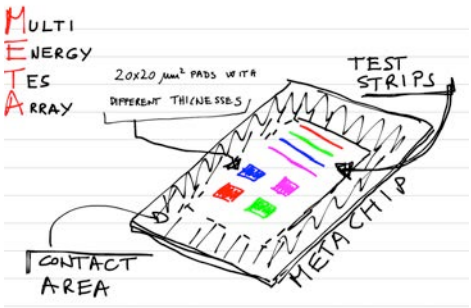

Figure 59 - META chip concept (see text).

The idea is to start with proven technology by INRIM (Ti-Au double-layer TES), and vary energy sensitivity by simply changing Au thickness. Four pads could initially cover the energy range 1 eV to 1 keV, and pads would be tested both individually and as an array. A potential problem to be investigated in the preliminary tests is phonon cross-talk between pads when working simultaneously on a wideband beam. The Trieste BaRBE group has received seed funding from INFN to start design and production of a prototype META chip in 2014.

3.2 CAST Physics motivation for axions, Chameleons or other WISPs

3.2.1 Solar axions with the forthcoming vacuum data taking run

CAST carried out its phase I, with vacuum in the magnet bores, in 2003 and 2004. The limit obtained to the axion-photon coupling $g_{a\gamma\gamma} < 8.8 \times 10^{-11}$ GeV^{-1}, (for $m_a < 0.02$ eV), the main result of CAST phase I, is now widely known and referenced by the community[14]. This value represents a factor of 6 in $g_{a\gamma\gamma}$ better than the previous axion helioscope (which translates into a factor of $>10^3$ better in the detectable signal strength -number of counts-). This limit is the first helioscope limit surpassing the stringent astrophysical bound $g_{a\gamma\gamma} < 10^{-10}$ GeV^{-1}, and entering previously unexplored ALP parameter space. Although vacuum operation of CAST does not provide sensitivity to QCD axion models (because of the lack of coherence for $m_a > 0.02$ eV, being this the motivation for phase II), the possibility of pushing CAST vacuum limit to lower $g_{a\gamma\gamma}$ values is also highly motivated, both theoretically and observationally. Technologically, CAST has now the possibility to operate in vacuum with increased sensitivity compared with our 2003/04 runs, based on recent ideas and developments that we are putting forward in the context of IAXO (the International Axion Observatory), the future axion helioscope whose Letter of Intent has been recently submitted to the SPSC. The tests of these ideas in CAST are *per se* motivated in view of the IAXO proposal.

These motivations were explained in detail in our proposal to SPSC of last year [9]. While we refer to that document for a complete description and a proper account of references, we will only briefly review them in the following points:

1) Although the axion is the best motivated and most studied prototype, a whole category of particles called axion-like particles (ALPs) or, more generically, weakly interacting slim particles (WISPs), is often invoked in several scenarios, theoretically well motivated[1]. Although not necessarily related with the axion, they share part of its phenomenology, and therefore they would be searchable by similar experiments. ALPs often appear in extensions of the SM as pseudo Nambu-Goldstone bosons of new symmetries broken at high energy. But most interestingly, string theory also predicts not just one ALP, but in most cases a rich spectrum of them (including the axion itself), something only recently realized and studied [15],[16]. Remarkably, the region of the ALP parameter space corresponding to the first orders of magnitude just beyond the current CAST bound in $g_{a\gamma\gamma}$ correspond to intermediate string scales and are specially motivated as they would contribute to the natural explanation of several hierarchy problems in the standard model (SM)

2) Another point worth noting is the possible connection between ALPs and dark matter (DM). Recently it has been noted that the non-thermal production mechanisms attributed to axions are indeed generic to ALPs (and to any bosonic WISP)[17]. The range of ALP parameters including ALP models possibly solving the DM problem gets substantially enlarged both in $g_{a\gamma\gamma}$ and m_a and in particular includes part of the region that an improved CAST vacuum run could probe, as shown in Figure 60.

3) A number of unexplained astrophysical observations may indicate the effects of an ALP. They must be treated with caution because usually an alternative explanation using standard physics or an uncontrolled systematic effect cannot be ruled out. One of them is the observation of VHE photons with directions correlated with very distant sources, apparently incompatible with the expected opacity of the intergalactic medium at such energies. Although not without controversy, this evidence might be supported by several independent observations. Different scenarios invoking photon-ALP oscillations triggered by intervening cosmic magnetic fields have been invoked by several authors to account for the unexplained observations. For some of these cases, approximate required ALP parameters $g_{a\gamma\gamma}$ and m_a are drawn. Interestingly, most of them coincide roughly in requiring very small ALP mass $m_a < 10^{-(10\text{-}7)}$ eV (to maintain coherence over sufficiently large magnetic lengths) and a $g_{a\gamma\gamma}$ coupling in the ballpark of $g_{a\gamma\gamma} \sim 10^{-12}$-$10^{-10}$ GeV^{-1}. These parameters are far from the standard QCD axions, however, as more generic ALP models, they lie just beyond the best current experimental limits on $g_{a\gamma\gamma}$ from CAST and are therefore feasible. They also roughly correspond to the parameters favored by string theory commented before. Any improvement beyond the current CAST vacuum limit will imply that part of this parameter space region would be probed.

4) Last but not least, the forthcoming vacuum run in CAST will test technological options that are proposed for the large-scale effort represented by IAXO. Two of the innovations in which CAST success has relied on are the use of x-ray focalization to increase the signal-to-noise ratio, and the use of low background techniques to reduce the detector backgrounds. The first strategy is exemplified by the CCD+ABRIXAS telescope detection line, while the second one by the other 3 detection line based on low background Micromegas detectors (with new results obtained this year, as explained in Section 2.2.1). Both options leading to similar final sensitivity. The new sunrise system to be completed next year will combine both strategies in the same system: a new x-ray optics coupled to a low background Micromegas detector. The implementation of this concept in CAST will not only increase the signal-to-noise ratio of the sunrise Micromegas, and the sensitivity of the experiment, but would serve as a pathfinder project to test the technological options being proposed to build large scale, cost effective, x-ray optics with customized parameters for the future IAXO.

The physics potential of our proposed 9-month data taking campaign in terms of sensitivity in the ALP ($g_{a\gamma\gamma}$-m_a) plane was presented in our SPSC report of last year [9], and is reproduced in Figure 60, compared with the current CAST limit $g_{a\gamma\gamma} < 8.8 \times 10^{-11}$ GeV^{-1} (for $m_a < 0.02$ eV). As shown, CAST could improve the current vacuum result down to $g_{a\gamma\gamma} < 5.9\text{-}6.3 \times 10^{-11}$ GeV^{-1}, corresponding to a factor 4-5 improvement in the detectable signal strength. This result would probe deeper into the unexplored ALP region motivated by the theoretical, cosmological and astrophysical arguments mentioned above. It is worth to note that the background assumptions made to compute the plot (described in the caption) are being proven realistic –and maybe even conservative- by the first commissioning results of the new Micromegas detector systems installed this summer (as described in Section 2.2.1).

In addition, in Figure 61, the expected exclusion limit (for $m_a < 0.02$ eV) is plotted for a variable exposure time of the experiment.

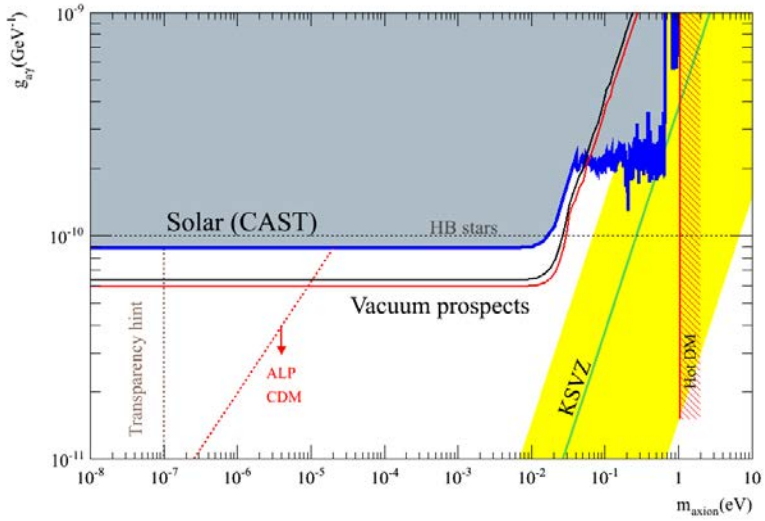

Figure 60 - Expected sensitivity with the setup proposed in vacuum conditions 9 calendar months assuming 75% data taking efficiency. Two assumptions in the background for the Micromegas detectors have been computed of 1.5×10^{-6} (black line) corresponding to a sensitivity of $g_{a\gamma\gamma} < 6.34 \times 10^{-11}$ GeV^{-1} and 8×10^{-7} counts keV^{-1} cm^{-2} s^{-1} (red line) with a sensitivity of $g_{a\gamma\gamma} < 5.94 \times 10^{-11}$ GeV^{-1}. The diagonal red dashed line represents the frontier of the parameter space region in which ALP models with a valid cold DM relic density can be found [17], while the region on the left of the vertical grey dashed line have been invoked in the solution of the Universe transparency problem as explained in the text.

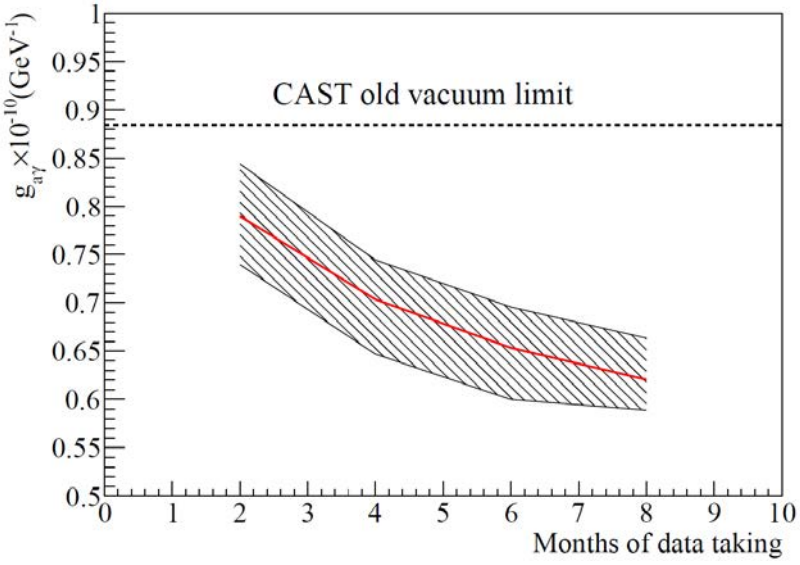

Figure 61 - Expected sensitivity to $g_{a\gamma\gamma}$ of the new CAST vacuum phase with the improved detectors, versus the exposure time of the data taking campaign. The dashed region represents the range of statistical fluctuations due to the low number of counts expected, computed as the range encompassing the results of 200 different simulations. The red line is the average result.

3.2.2 Solar Chameleons

The dark matter problem could be solved by theoretically motivated particles such as axions, WIMPs, etc. However, the problem of the dark energy (DE) lacks such well-motivated

solutions, while the greatest mystery in modern cosmology is the origin of the accelerating expansion of our universe, suggesting some "*new physics*" behind this observation. CAST offers a window of opportunity also for DE particle identification at the elementary level. We recall, the cosmic acceleration has been observed using cosmological probes, which constrain its large-scale behaviour. It is this that makes laboratory experiments in this field so attractive, and in particular if they can be operated without interfering with the rest of the research program; this is the case for CAST, aiming eventually to pin down the underlying microphysics.

The motivation for solar chameleons along with the estimated CAST sensitivity to such particles has been presented last year in the report to SPSC [9]. From the already reached detection performance of solar chameleons via their coupling to photons (β_γ) [and soon hopefully also to matter (β_m)], we are already not far from the expectations of last year. Thus, for 2013-2014, assuming a larger surface SDD and a low threshold InGRID detector attached alternatively at the focal plane of the X-ray telescope (XRT), CAST has the potential to remain in the forefront as lab experiment searching for chameleons or other similar particles from the Sun. Therefore, we can now make safer projections into the (near) future for both approaches. I.e., a) via the Primakoff-effect, and b) via their radiation pressure when chameleons get reflected off a dense membrane inside an opto-mechanical cavity, which is a novel and interdisciplinary concept.

CAST is presently the only helioscope searching for solar axions, chameleons or other ALPS. The scheduled new vacuum measurements with CAST have started already, and the better performing detectors after so many years of experience, allow us to expect a better sensitivity for solar axions or ALPS with rest mass below ~0.02 eV/c^2. With data started taking already in the sub-keV range, for the first time for a helioscope like CAST, we enter into an unexplored domain.

In addition, the X-ray detector in the focal plane of the CAST-XRT can be replaced by a radiation pressure sensor being currently fine tuned in Trieste. We aim at reaching the nominal sensitivity [18] mentioned in the last report to SPSC [9]. The importance of such a novel measurement is that its envisaged sensitivity goes via the matter coupling of the chameleon field. With such a measurement, we may reach a unique direct detection method for fields like chameleons, if their coupling depends *only* on the environmental matter-energy density. With this scheme, CAST has the potential to be sensitive to a solar chameleon luminosity far below the one expected to be seen by detectors, which are sensitive to soft X-rays coming from Chameleon-photon oscillations in the source [=Sun's magnetic field] and in the magnetic pipes of CAST.

Though, competitive experiments may show-up any time, and CAST is exploiting its full potential in future. The recent dish antenna idea [19] is just an example, which might change the landscape of our field. Therefore, we present below[20] the potential utilization of this new concept in CAST.

3.2.3 New perspective: CAST as a tracking haloscope for relics

According to the idea of the "dish antenna"[19], dark matter axions or ALPS could convert to photons when hitting a mirror antenna, which has to be inside a magnetic field (B) oriented along the mirror surface. The expected performance of this technique has been widely recognised, and it looks impressive as we witnessed it, e.g., in the last Patras workshop in Mainz/Germany. Interestingly, beyond the ongoing activities in DESY, also the Japanese axion helioscope SUMICO intends to apply this approach. Similarly, this possibility has been included also by IAXO in the LoI to SPSC. The simplicity of the idea allows one to assume that also others (will) follow this concept. We looked into this idea[20] following the CAST configuration. The general outcome seems double attractive for CAST becoming a tracking axion haloscope.

In fact, the relic axion/ALP signal is proportional to $\mathbf{A \cdot B^2 \cdot (g_{a\gamma\gamma})^2}$ (**A** is the antenna surface area). Then, using the results presented in [19], we approximately scale down using the corresponding values relevant for CAST, i.e., A = 10 cm^2 and B = 9 T. This implies, by comparison, CAST can be sensitive to relic ALPS with a sensitivity to a coupling constant being larger by a factor of ~20. To put it differently, in a rest mass range 10^{-6} eV/c^2 to 10^{-4} eV/c^2, the potential improvement, of the current world best limit measured by CAST, can be improved by a factor of ~1000 to ~50, respectively. An extrapolation towards higher rest masses seems reasonable. This is an essential improvement, and therefore it deserves a rigorous investigation of all factors entering in the overall performance.

In addition, the CAST tracking possibility might open a new window towards detecting streaming dark matter with an eventually enhanced sensitivity [20]. To implement this additional idea, once CAST operates as an axion/ALPS haloscope, it requires no new equipment.

CAST has thus the perspective to become *the first tracking haloscope* of relic axions/ALPS with a good sensitivity and discovery reach. Quantitative estimates are in progress, in order to decide about such an upgrade of CAST. Collaboration with DESY, where the dish antenna idea came-up, but also with other astrophysics laboratories (with experience in detectors in the relevant frequency band), seems necessary for the realization of such a project.

3.3 Planned schedule and requests for 2014

In view of the delay in recalibrating the MPE-XRT at PANTER until at least the 19th November, and given that there is no longer a possibility to install & align the XRT before the end of the 2013 run, CAST has decided to install the XRT at the start of 2014.

CAST now plans to take data with the SSMM, SRMM and SDD until the end of the run (~10 December 2013). The schedule until the end of the run is shown in Figure 62.

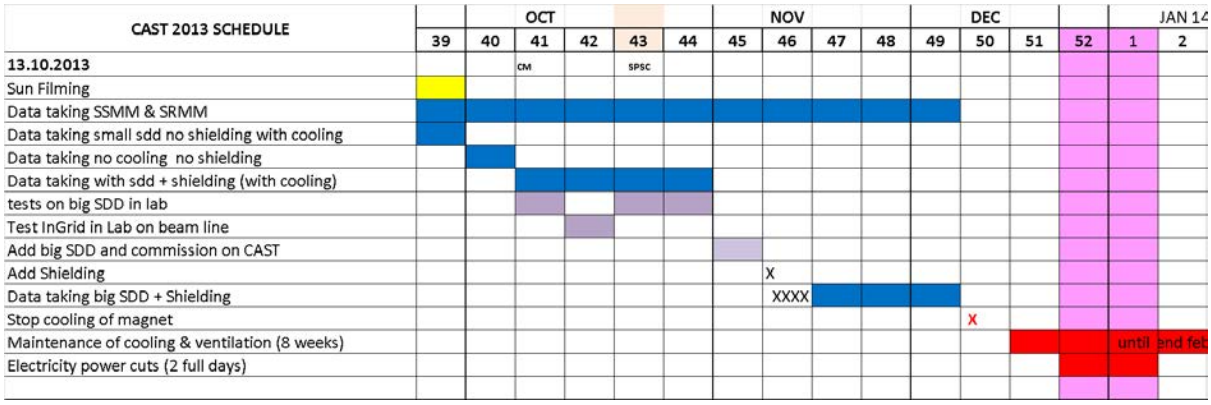

Figure 62 - Schedule to end of 2013.

The winter shutdown of CAST will contain the usual cryogenics and vacuum maintenance. The start of the cool-down of the CAST magnet depends on LS1 activities. CAST originally requested 1st April for start of cryogenics, we have since requested to start in mid-March 2014 but no confirmation so far received.

There are no large-scale interventions planned for the shutdown. The infrastructure for the final setup of the SRMM and LLNL-XRT beam line will be installed and the infrastructure for the InGrid and BaRBE detector sub-systems will be installed.

The present schedule for 2014 contains (see Figure 63):

- Install InGrid infrastructure
- Dismount SSMM and SDD
- Install and align MPE-XRT
- Install InGrid (and BaRBE)
- Align InGrid
- Sun filming possible?
- Cool down magnet
- Magnet cold
- Quench tests
- Install LLNL –XRT
- Align LLNL-XRT
- Install SRMM and check alignment
- Check alignment MPE-XRT /INGRID/BaRBE magnet cold
- Install SSMM
- GRID
- Start data taking

In 2014 there should be 6 months data taking with two XRT's and an InGrid detector capable of sub-keV operation.

Present Schedule 2014												
2014	**JAN**	**FEB**	**MAR**	**APR**	**MAY**	**JUN**	**JUL**	**AUG**	**SEP**	**OCT**	**NOV**	**DEC**
Remove SSMM	XX											
InGrid (Barbe)												
Install InGrid infrastructure												
Install XRT		X										
Align XRT(magnet warm)		XX										
Install Ingrid (")		X										
Align InGrid (")			X									
Align Barbe ? (")			XX									
Magnet & Sun filming												
Cool Down magnet *(depends on LHC infrastructure- could be later)*			X	X								
SUN FILMING ? Not Possible if magnet inbetween 300 & 1.8K			?									
Magnet cold				X								
Magnet tests (quench)				X								
SR Line												
CALIBRATE LLNL-XRT												
Dismount SR line												
Install LLNL XRT				XX								
Align LLNL XRT				X	X							
Check alignment of MPE-XRT					X							
Install SRMM					X							
Install SSMM					X							
GRID						X						
DATA TAKING						XXX						X

Figure 63 – Present CAST schedule for 2014. The KWISP Radiation Pressure force sensor prototype (see Section 3.1.3) will be tested in Trieste in October-November 2013. The commissioning in the XRT focal plane can be foreseen for March-April 2014.

Estimates for the Cryo Operations (M&O) costs in kCHF, running hours, electricity power. Costs (cryogenics and power converter) and costs for the FSU contract for the power converter are shown in Figure 64.

			Actual values		Projected values	
Item	**Dept**		**2011**	**2012**	**2013**	**2014**
		Units				
Cryogenics M&O	**EN**	(kCHF)	**180**	**180**	**180**	**180**
Cryogenics power	**EN**	*(hours)* **(kCHF)**	*2951* **81**	*4877* **134**	3696 **102**	*6570* **181**
Power Converter power	**EN**	*(hours)* **(kCHF)**	*797* **6**	*1576* **11**	1232 **9**	*2168* **16**
FSU maintenance (TE)	**CAST**	(kCHF)	5	5	5	5
Yearly TOTAL	**CERN**	**(kCHF)**	**267**	**325**	**290**	**376**

Figure 64 - Magnet support costs, estimates for 2013 and 2014.

CAST requests from CERN continued support at a similar level to the past years, namely:

PH-DT Consultant Mechanical engineer. Mechanical technician - support for the experimental apparatus including movement system.

Electrical technician - support for Slow Control and interlocks and electrical support for SDD.

Applied Fellow. Completion of the 3He CFD project, liaison with EN-CV, x-ray test lab and SDD.

TE-VSC Consultant vacuum physicist/technician.

Aid with the interventions on magnet and detector vacuum systems and in x-ray lab.

TE-EPC Support for the Power Converter (PC) operation and maintenance.

TE-CRG	Cryolab support for measures to place and maintain 3He system on Standby during vacuum running. Help with dismounting and re-mounting and all manipulation of cryo sensors. Support for the maintenance the 3He system PLC for at least one year after end of 4He run. Support for the operation of the magnet cryogenics and its ABB control system Support for opening and closing the cryostat to change cold windows
TE-MPE	Support for the Quench Protection rack
EN-ICE	Support for the Power Converter controls system
BE-ABP	General Survey work and support for the alignment of two X-ray telescopes
EN-MME	Coordination of integration of detectors and telescopes on XRT platform
TE-CV	Support for demineralized water cooling system for 13 kA cables and Power Converter. Support for completion of 3He CFD simulations

4 Conclusions

The measurements in vacuum being performed under lower detector background have the potential, in case of no signature, to improve CAST own world best limit for solar ALPS below ~20 meV/c^2.

The already started CAST data taking for solar chameleon searches in the sub-keV range is based on the Primakoff – effect. CAST became thus one among few laboratory experiments worldwide operating in the territory of the dark energy sector. Low energy threshold detectors are the key in making CAST the first and best performing solar helioscope for particles like Chameleons.

In addition, a novel interdisciplinary radiation pressure concept was used to build a force sensor, with tests being in progress. This entirely in-house-made state-of-the-art force sensitive device can be installed in CAST by replacing alternatively the sub-keV X-ray detector at the focal plane of the XRT. Interestingly, measurements with the force sensor could be performed also parasitically in periods when the CAST magnet is, for some reason, temporarily unavailable.

Then, CAST may not end with its present basic program on solar ALPS and Chameleons.

[1] J. Jaeckel and A. Ringwald, *The Low-Energy Frontier of Particle Physics*, Annual Review of Nuclear and Particle Science 60 (Nov., 2010) 405–437.
[2] A. Ringwald, *Ultralight Particle Dark Matter*, arXiv:1310.1256.
[3] G. Cantatore, M. Karuza, V. Lozza, and G. Raiteri, Nucl. Instr. and Meth. A, 617 502-504 (2010).
[4] M. Arik et al. [CAST Collaboration], arXiv:1307.1985.
[5] K. Barth et al., *CAST constraints on the axion-electron coupling*, JCAP 1305 (2013) 010.
[6] T. Mizumoto et al., JCAP 07 (2013) 013.
[7] H. An, M. Pospelov and J. Pradler, arXiv:1309.6599.
[8] F. A. Harrison et al. (*NuSTAR* Collaboration), "The Nuclear Spectroscopic Telescope Array (*NuSTAR*) Mission," *ApJ* **770**, 103 (2013), [arXiv:astro-ph/1301.7307].
[9] T. Papaevangelou, Status report of the CAST Experiment, CERN-SPSC-2012-028 / SPSC-SR-106 11/10/2012.
[10] M. Karuza et al., *Optomechanical sideband cooling of a thin membrane within a cavity*, New J. Phys. 14, 095015 (2012).
[11] A 50 nm thick, (1 mm)x(1 mm) silicon nitride window (micro-membrane) made by Norcada, http://www.norcada.com.
[12] In collaboration with G. Di Giuseppe, R. Natali and A. Vitali.
[13] Istituto Nazionale RIcerca Metrologica, Torino. TES chips made by E. Monticone and M. Raiteri.
[14] K. Zioutas et al. [CAST Collaboration], *First results from the CERN Axion Solar Telescope (CAST)* Phys. Rev. Lett. 94, 121301 (2005) [hep-ex/0411033].
[15] M. Cicoli, M. Goodsell, and A. Ringwald, The type IIB string axiverse and its low-energy phenomenology, arXiv:1206.0819.
[16] A. Ringwald, Searching for axions and ALPs from string theory, arXiv:1209.2299.
[17] P. Arias, D. Cadamuro, M. Goodsell, J. Jaeckel, J. Redondo, *et. al*., *WISPy Cold Dark Matter*, arXiv:1201.5902.
[18] In collaboration with A. Lindner, Y.K. Semertzidis and A. Upadhye.
[19] D. Horns, J. Jaeckel, A. Lindner, A. Lobanov, J. Redondo, A. Ringwald, JCAP 1304 (2013) 016.
[20] D.H.H. Hoffmann, A. Lindner, K. Zioutas, in preparation (2013).